A subset of brain regions within adult functional connectivity networks demonstrate high reliability across early development

Authors:
Jiaxin Cindy Tu[1], Yu Wang[2], Xintian Wang[1], Donna Dierker[1], Chloe M. Sobolewski[1,3], Trevor K. M. Day[4,5,6], Omid Kardan[7], Óscar Miranda-Domínguez[4], Lucille A. Moore[4], Jed T. Elison[4,5], Evan M. Gordon[1], Timothy O. Laumann[1], Adam T. Eggebrecht[1], Muriah D. Wheelock[1]

Affiliations:
[1]Department of Radiology, Washington University in St. Louis.
[2]Department of Mathematics and Statistics, Washington University in St. Louis.
[3]Department of Psychology, Virginia Commonwealth University.
[4]Masonic Institute for the Developing Brain, University of Minnesota.
[5]Institute of Child Development, University of Minnesota.
[6]Center for Brain Plasticity and Recovery, Georgetown University.
[7]Department of Psychiatry, University of Michigan.

Corresponding Author
Muriah D. Wheelock
Mallinckrodt Institute of Radiology
4525 Scott Ave
St. Louis, MO 63110
mdwheelock@wustl.edu

Highlights

- Specialized functional networks in the human cerebral cortex, evident in resting-state fMRI, support sensory, motor, cognitive, and affective functions and evolve throughout the lifespan.
- Existing studies have focused on age-specific networks for infants, but less on to what extent adult networks can describe infant functional connectivity (FC).
- Analysis revealed a subset of areas in infants showing adult-like network organization, with within-network FC exhibiting less variation across age and higher reliability across scans.
- These areas are posited near locations with low variability in functional network identity in adults, suggestive of the relationship between developmental sequence and interindividual variability in functional network organization.

Keywords
fMRI, functional connectivity, system, network, infant, resting state

Abstract

The human cerebral cortex contains groups of areas that support sensory, motor, cognitive, and affective functions, often categorized as functional networks. These areas show stronger internal and weaker external functional connectivity (FC) and exhibit similar FC profiles within rather than between networks. Previous studies have demonstrated the development of these networks from nascent forms present before birth to their mature, adult-like topography in childhood. However, analyses often still use definitions based on adult functional networks. We aim to assess how this might lead to the misidentification of functional networks and explore potential consequences and solutions.

Our findings suggest that even though adult networks provide only a marginally better than-chance description of the infant FC organization, misidentification was largely driven by specific areas. By restricting functional networks to areas showing adult-like network clustering, we observed consistent within-network FC both within and across scans and throughout development. Additionally, these areas were spatially closer to locations with low variability in network identity among adults. Our analysis aids in understanding the potential consequences of using adult networks "as is" and provides guidance for future research on selecting and utilizing functional network models based on the research question and scenario.

1. Introduction

At the meso-scale, the human cerebral cortex consists of specialized functional modules (Power et al., 2011; Yeo et al., 2011) that work together as large-scale functional networks to support sensory, motor, higher-cognitive, and affective functions (Petersen & Sporns, 2015; Wig, 2017). In adult humans, these large-scale networks exhibit relatively consistent spatial topographies across both acquisition paradigms (task and resting states) and individuals (Gratton et al., 2018), and are disrupted by disease (Fornito et al., 2015; Fox & Greicius, 2010). The modular composition of the brain serves to segregate information processing between distinct sensory modalities or cognitive domains (Grayson & Fair, 2017; Petersen & Sporns, 2015).

Prior research has demonstrated that these functional networks develop across the lifespan from infancy through old age (Grayson & Fair, 2017; Sun et al., 2023; Wig, 2017), paralleling the development of complex behavior functions (Grayson & Fair, 2017; Petersen & Sporns, 2015). Preliminary forms of adult functional networks are already present in utero (Moore et al., 2024; Thomason et al., 2013; Turk et al., 2019). In addition, the existence of robust, bilateral segregated networks for somatomotor, primary auditory, primary visual, and extrastriate visual cortex have also been confirmed (Eyre et al., 2021; Fransson et al., 2007; Gao, Alcauter, Elton, et al., 2015, 2015; Smyser et al., 2010). Higher-order resting-state networks appear to be less mature in early infancy (Gao, Alcauter, Elton, et al., 2015; Gao et al., 2009). By the age of 1-2 years, the default mode network becomes more adult-like in some studies (Gao, Alcauter, Elton, et al., 2015; Gao, Alcauter, Smith, et al., 2015; Gao et al., 2009) but remains localized in other studies (Eggebrecht et al., 2017; Kardan et al., 2022; Marrus et al., 2018; F. Wang et al., 2023).

Due to these observations, researchers conducting analysis on infant neuroimaging data often face a dilemma of choosing a proper representation model for

their data. Some researchers used the adult network models when describing the relationships between functional connectivity (FC) in the brain and behavioral phenotypes in infants (Nielsen et al., 2022; Rudolph et al., 2018; Tooley et al., 2023) or when comparing between infants and adults (Yates et al., 2023). One argument for this choice is to encourage biological interpretability and facilitate communication across groups by adopting the same terminology across developmental stages. However, defining the functional networks using the exact adult topography may be inaccurate and cause the mixing of fMRI BOLD signals across different sub-networks (Smith et al., 2011), thus lowering statistical power. Furthermore, some of the differences in FC might be confounded by the differences in network topography or network identity (Bijsterbosch et al., 2018, 2019).

An alternative approach is to derive data-driven functional networks for specific developmental stages (Eggebrecht et al., 2017; Kardan et al., 2022; Marrus et al., 2018; Wheelock et al., 2019). While this would potentially mitigate the problem of poor FC representation within functional networks and help improve reproducibility, the utility and interpretability of those results are less apparent. Ultimately, the choice should be dependent on the research goal, but it is also important to understand how poorly the adult network topography fits data from infants – presumably, if the adult functional network topography is dramatically different from that in infants, then the application of the adult functional networks to infant studies would likely result in low reliability (Marek et al., 2022). Here, we aim to delve deeper into this problem, and examine to what extent the infant networks are similar to and different from the adult networks in terms of describing the underlying modular structure in their FC.

In addition, converging evidence from different modalities suggests that the human cortex does not develop in a spatially uniform manner. Rather, regions within primary sensory and motor cortex mature earlier in their biological properties than regions in higher order association cortex (Ahmad et al., 2023; Flechsig, 1901; Garcia et al., 2018; Grayson & Fair, 2017; Hill et al., 2010; Sydnor et al., 2021; Truzzi & Cusack, 2023). When the areas mature earlier, it leaves little room for future plasticity (Hill et al., 2010), and hence may result in less interindividual variability or reduced susceptibility to environmental influences (Gao et al., 2017) and psychopathological factors (Sydnor et al., 2021). We hypothesized that some areas would demonstrate early signs of adult-like organization, especially towards the sensorimotor end of the functional hierarchy (Gao, Alcauter, Elton, et al., 2015; Sydnor et al., 2021). We further hypothesized that areas with adult-like organization would overlap with areas of low interindividual variability in functional network assignments (Dworetsky et al., 2021; Gordon, Laumann, Adeyemo, et al., 2017; Gratton et al., 2018; Hermosillo et al., 2024; Kong et al., 2019; Langs et al., 2016; Seitzman et al., 2019).

In the present work, we used one adult resting-state fMRI dataset with 120 participants (aged 19-32 years) and one typically developing infant resting-state fMRI dataset with 181 participants (aged 8-60 months) to quantify how well the infant and adult networks can describe the modular structure in the adult and infant FC. In addition, we quantified the fit of the networks in each area and mapped out the spatial distribution of the strength of misidentification. Furthermore, we analyzed the age effect on within-network FC using all areas versus only the subset of areas with a stronger association to other areas in the same network than alternative networks to

demonstrate the potential consequences of model choice. Lastly, we compared the spatial distribution of our area subset to the spatial distribution of locations with the greatest group convergence in functional network identity across individuals. Our findings will help researchers working with infant neuroimaging data understand the pros and cons of using adult and infant functional network models, appreciate the current results in the literature, and provide recommendations for future research.

2. Materials and Methods

2.1. Data Collection

2.1.1. Washington University 120 (WU 120)

This dataset has been previously described in detail (Power et al., 2017). Briefly, data were collected from 120 healthy young adult subjects during relaxed eyes–open fixation (60 females, mean age = 25 years, age range = 19–32 years). All subjects were native speakers of English and right-handed. Subjects were recruited from the Washington University community and were screened with a self-report questionnaire to ensure that they had no current or previous history of neurological or psychiatric diagnosis, as well as no head injuries resulting in a loss of consciousness for more than 5 minutes. Informed consent was obtained from all subjects. The study was approved by the Washington University School of Medicine Human Studies Committee and Institutional Review Board.

Structural and functional MRI data were obtained with a Siemens MAGNETOM Trio Tim 3.0-T Scanner (Erlangen, Germany) and a Siemens 12-channel Head Matrix Coil. A T1-weighted sagittal magnetization-prepared rapid acquisition gradient-echo (MP-RAGE) structural image was obtained [time echo (TE) = 3.08 ms, time repetition, TR (partition) = 2.4 s, time to inversion (TI) = 1000 ms, flip angle = 8°, 176 slices with 1 × 1 × 1 mm voxels]. An auto-align pulse sequence protocol provided in the Siemens software was used to align the acquisition slices of the functional scans parallel to the anterior commissure–posterior commissure plane of the MP-RAGE and centered on the brain. This plane is parallel to the slices in the Talairach atlas (Talairach & Tournoux, 1988).

During functional MRI data acquisition, subjects were instructed to relax while fixating on a black crosshair that was presented against a white background. Functional imaging was performed using a BOLD contrast-sensitive gradient-echo echo-planar imaging (EPI) sequence (TE = 27 ms, flip angle = 90°, in-plane resolution = 4 × 4 mm). Whole-brain EPI volumes (MR frames) of 32 contiguous, 4-mm-thick axial slices were obtained every 2.5 s. A T2-weighted turbo spin-echo structural image (TE = 84 ms, TR = 6.8 s, 32 slices with 1 × 1 × 4 mm voxels) in the same anatomical planes as the BOLD images was also obtained to improve alignment to an atlas. Anterior→Posterior (AP) phase encoding was used for fMRI acquisition. The number of volumes collected from subjects ranged from 184 to 724 (mean = 336 frames, 14.0 min).

2.1.2. Baby Connectome Project (BCP)

Full-term (gestational age of 37-42 weeks) infants free of any major pregnancy and delivery complications were recruited as part of the Baby Connectome Project

(Howell et al., 2019). All procedures were approved by the University of North Carolina at Chapel Hill and the University of Minnesota Institutional Review Boards. Informed consent was obtained from the parents of all participants. In the final cohort used following fMRI data quality control (described below), we retained 313 MRI sessions from 181 individuals (95 females, 8-60 months, mean 19.1 months and standard deviation 8.3 months) (Supplementary Figure 1).

All MRI images were acquired on a Siemens 3T Prisma scanner with a 32-channel head coil at the University of Minnesota and at the University of North Carolina at Chapel Hill during natural sleep without the use of sedating medications. T1-weighted (TR=2400 ms, TE=2.24 ms, 0.8 mm isotropic; flip angle = 8°), T2-weighted images (TR=3200 ms, TE=564 ms, 0.8 mm isotropic), spin echo field maps (SEFM) (TR=8000 ms, TE=66 ms, 2 mm isotropic, MB=1), and fMRI data (TR=800 ms, TE=37 ms, 2 mm isotropic, MB=8) were collected. A mixture of Anterior→Posterior (AP) and Posterior→Anterior (PA) phase encoding directions was used for fMRI acquisition in each session, but they were concatenated into one time series. An early subset of data was collected with a 720-ms TR (N = 95). The number of low-motion volumes collected from subjects ranged from 840 to 2100 (mean = 1306 frames, 16.9 min).

2.2. fMRI analysis

2.2.1. MRI data preprocessing

2.2.1.1. MRI data preprocessing – WU120

Functional images were first processed to reduce artifacts including (1) Correction of odd versus even slice intensity differences attributable to interleaved acquisition without gaps, (2) correction for head movement within and across runs, and (3) across-run intensity normalization to a whole-brain mode value of 1000. Atlas transformation of the functional data was computed for each individual using the MP-RAGE scan. Each run was then resampled to an isotropic 3-mm atlas space (Talairach & Tournoux, 1988), combining movement correction and atlas transformation in a single cubic spline interpolation (Lancaster et al., 1995).

Additional preprocessing steps were applied to the functional data to reduce the effect of high-motion frames. This was performed in two iterations. In the first iteration, the processing steps were (1) demeaning and detrending, (2), multiple regression including: whole-brain, ventricular cerebrospinal fluid (CSF), and white matter signals, and motion regressors derived by Volterra expansion and (3) a band-pass filter (0.009 Hz < f < 0.08 Hz). Following the initial FC preprocessing iteration, temporal masks were created to flag motion-contaminated frames. Motion-contaminated volumes were identified by framewise displacement (FD), defined as the squared sum of the motion vectors (Power et al., 2012). Volumes with FD > 0.2 mm and segments of data lasting fewer than 5 contiguous volumes were censored.

The data were then reprocessed in a second iteration, incorporating the temporal masks described above. This reprocessing was identical to the initial processing stream but ignored censored data. Data were interpolated across censored frames using least squares spectral estimation (Power et al., 2014) of the values at censored frames, so that continuous data could be passed through the band-pass filter (0.009 Hz < f < 0.08

Hz) without contaminating frames near high motion frames. Censored frames were ultimately ignored during functional connectivity matrix generation.

Individual surfaces were generated from the structural images and the functional data was sampled to surface space (Glasser et al., 2013). First, following volumetric registration, anatomical surfaces for the left and right hemispheres were generated from each subject's MP-RAGE image using FreeSurfer's default recon-all processing pipeline (v5.0)(Fischl, 2012). This pipeline included brain extraction, segmentation, generation of white matter and pial surfaces, inflation of the surfaces to a sphere, and surface shape-based spherical registration of the subject's "native" surface to the fsaverage surface. The fsaverage-registered left and right hemisphere surfaces were then brought into register with each other (Van Essen et al., 2012), resampled to a resolution of 164000 vertices using Caret tools (Van Essen et al., 2001) and subsequently down sampled to a 32492 vertex surface (fs_LR 32k). The BOLD volumes were sampled to each subject's individual "native" midthickness surface (generated as the average of the white and pial surfaces) using the ribbon-constrained sampling procedure available in Connectome Workbench (v0.84) and then deformed and resampled from the individual's "native" surface to the 32k fs_LR surface. Finally, the time courses were smoothed along the 32k fs_LR surface using a Gaussian smoothing kernel (σ = 2.55 mm).

2.2.1.2. MRI data preprocessing – BCP

MRI data were processed using the DCAN-Labs infant-abcd-bids-pipeline (v0.0.22) largely following steps described previously (Feczko et al., 2021). Structural MRI data underwent HCP-style processing (Feczko et al., 2021; Glasser et al., 2013), including ANTS N4 bias correction, ANTS denoising, T1/T2 distortion correction/registration, and finally ANTS SyN algorithm deformation alignment to an infant MNI template. In addition, a refined brain mask was generated from data that was segmented using in-house age-specific templates via Joint Label Fusion (JLF). The toddler-specific mask and segmentation were substituted into the FreeSurfer (Fischl, 2012) pipeline and used to refine the white matter segmentation and guide the FreeSurfer surface delineation. The native surface data were then deformed to the fsaverage LR32k template via a spherical registration.

For functional MRI preprocessing, a scout image (frame 16 in each run) was selected from the fMRI time series. The scout was distortion-corrected via spin-echo field maps, served as the reference for motion correction via rigid-body realignment (Feczko et al., 2021), and was registered to the native T1. Across-run intensity normalization to a whole-brain mode value of 10,000 was then performed. These steps were combined in a single resampling with the MNI template transformation from the previous step, such that all fMRI frames were registered to the infant MNI template. Manual inspection of image quality of structural and functional data was conducted to exclude sessions with bad data quality.

To prepare the functional data for FC analysis, further processing steps were applied after sampling the BOLD data to the fsLR_32k surface space using steps described in 2.2.1.1. First, functional data were demeaned and detrended in time. Denoising was then performed using a general linear model with regressors including signal and motion variables. Signal regressors included mean CIFTI gray-ordinate time

series, Joint Label Fusion (JLF)-defined white matter, and JLF-defined CSF. Motion regressors included volume-based translational and rotational components and their 24-parameter Volterra expansion. The movement of the head was measured by FD and an age-specific respiratory notch filter (0.28-0.48 Hz) was applied to the FD traces and motion parameter estimates to mitigate the effects of factitious head motion due to infant respiration (Fair, 2020; Kaplan et al., 2022). Frames were censored during demeaning/detrending if their post-respiratory filtering FD value exceeded 0.3 mm to generate the denoised beta values in the general linear model. Bandpass filtering was applied using a second-order Butterworth filter (0.008–0.09 Hz). To preserve the temporal sequence and avoid aliasing caused by missing time points during bandpass filtering, interpolation was used to replace missing frames, and residuals were acquired from the denoising general linear model. In addition, zero-padding was applied to both ends of the BOLD data prior to filtering to minimize the distortions in the edges of the time series. The data were originally minimally spatially smoothed with a geodesic 2D Gaussian kernel (σ = 0.85 mm). A further smoothing with a geodesic 2D Gaussian kernel (σ = 2.40 mm) was applied to give a final effective smoothing of σ = 2.55 mm to match the smoothing used in the adult dataset (WU 120). Finally, the timeseries were concatenated across all complete and partially completed scan runs with good data quality. The first 7 frames from each run, frames with > 0.2 mm FD post-respiratory filtering (Kaplan et al., 2022) and outlier frames whose across-vertex standard deviation was more than 3 median absolute deviations from the median of the low FD frames were censored and ignored for functional connectivity matrix construction.

2.2.2. Functional Connectivity Matrix Construction

The preprocessed BOLD timeseries data of each session were parcellated into 333 non-overlapping areas using the Gordon parcellation (Gordon et al., 2016). This choice of parcellation was justified by recent work by our group that demonstrated that the Gordon parcellation had the best fit among a set of adult parcellations and performed comparably to most available infant parcellations in data from infants aged around 8-30 months (Tu et al., 2023). After that, a total number of frames equivalent to 7.2 minutes of data (560 frames for TR = 0.72 and 600 frames for TR = 0.8) were randomly sampled from the full censored timeseries in each fMRI session. The Pearson's correlation between the parcellated timeseries was computed to create a 333 x 333 functional connectivity (FC) matrix. This matrix was then Fisher-Z-transformed. The group-average FC matrix was calculated as the mean FC across fMRI sessions.

2.3. Infant and Adult Functional Networks Schemes

We used the Gordon network assignments (Gordon et al., 2016) for "Adult Networks" (Figure 1A) and Kardan network assignments (Kardan et al., 2022) for "Infant Networks" (Figure 1B). These networks were derived at the 333 area level using the same Infomap community detection algorithm (Rosvall & Bergstrom, 2010) optimized for identifying networks in FC data (Power et al., 2011). Among the 333 areas, some were originally assigned in communities fewer than 5 areas and considered unassigned (named "None" and "Unspecified"). These areas commonly fall under locations subjected to the biggest susceptibility artifact (Ojemann et al., 1997). We removed them

from all analyses and had 286 areas left for the adult networks ("Gordon") and 328 areas left for the infant networks ("Kardan").

The 12 Gordon networks include the auditory (Aud), cingulo-opercular (CON), parietal memory (PMN), default mode (DMN), dorsal attention (DAN), fronto-parietal (FPN), retrosplenial temporal (RTN), somatomotor hand (SMN hand), somatomotor mouth (SMN mouth), salience (Sal), ventral attention (VAN), and visual (Vis) networks. The 10 Kardan networks include somatomotor (SMN), temporal (Tem), posterior frontoparietal (pFPN), posterior default mode (pDMN), lateral visual (lVis), medial visual (mVis), dorsal attention (DAN), anterior fronto-parietal (aFPN), anterior default mode (aDMN).

2.4. Functional Network Overlap

The overlap between a network in the Gordon networks and a network in the Kardan networks can be measured with the Dice coefficient, with 0 indicating no overlap and 1 indicating complete overlap. For this analysis, each network is represented with a 333 x 1 vector with 1 for the areas in the network and 0 for the areas outside the network.

2.5. Silhouette Index Calculation

Following prior procedures in the literature (Rousseeuw, 1987; Yeo et al., 2011), we calculated the silhouette index (SI) for each area with the correlation distance using the spatial similarity between the FC profiles (without the diagonal elements which refer to the meaningless self-connectivity):

$$SI = \frac{b - a}{\max(a, b)} \quad (Equation\ 1)$$

where *b* is the mean between-network correlation distance of the FC profiles, and *a* is the mean within-network correlation distance of the FC profiles. FC profiles here refer to the FC from each area to all other areas (i.e., one row in the FC matrix).

Intuitively, the SI ranges from +1 to -1 with the sign indicating whether the area has a more similar FC profile to areas in its own network (+) or to areas in an alternative network (-). The magnitude indicates the confidence of this assignment, with a higher magnitude suggestive of strong confidence. The average SI for the FC in a network scheme was defined as the average SI across all areas.

By default, the silhouette index compares the current network to the best alternative network, which also depends on the quality of alternatives. However, other researchers have chosen to use a similar metric that compares the average within-network similarity to the average between-network similarity across all alternative networks, rather than just the best alternative (Ji et al., 2019). This approach tends to be less conservative and generally results in a higher silhouette index when calculated in this manner. We also calculated the silhouette index with the average of all networks rather than just the alternative network in the Supplementary Materials.

In order to obtain a confidence interval for the average SI across individual sessions, we used a bootstrap 95% confidence interval estimate in 1000 random draws

of individual sessions from the full sample (N = 120 for WU120 and N = 313 for BCP) with replacement.

2.6. Identify the Subset of Areas with Similar Network Organization to the Gordon Networks in Infants

A positive SI indicates that the area has a more similar FC profile to areas in its own network. We obtained the subset of areas that had a similar network organization to other areas defined in the Gordon network scheme in infants by only retaining the areas with a positive SI in the group-average infant FC. We refer to this set of positive SI areas as 'Gordon Subset'.

2.7. Distance Between High Consensus Regions of Interests (ROIs) and the "Gordon Subset" Areas

To quantify the spatial distribution similarity between the locations of low interindividual variability and the "Gordon Subset" areas, we calculated the Euclidean distance between the high consensus cortical ROIs and the centers of the Gordon areas. We used published coordinates of 153 high consensus ROIs calculated previously by identifying locations that demonstrated consistent network assignment across a large majority (i.e. ≥ 75%) of subjects in the Dartmouth dataset (N = 69 subjects, 56 female, average age 20.2 years)(Gordon et al., 2016) when a template-matching procedure (Gordon, Laumann, Adeyemo, et al., 2017) was applied to identify individual network assignments (Dworetsky et al., 2021).

For each of the "high consensus" ROIs, we found their distance to the nearest "Gordon Subset" area and their distance to an alternative Gordon area. An average of this difference was recorded and named "distance difference". A negative distance difference indicates that on average, the high consensus regions were closer to the "Gordon Subset" area centers than to the alternative Gordon areas. To account for the potential effect of differences in number of areas between the "Gordon Subset" areas (N = 166) and the alternative areas not in the subset (N = 120), we randomly assigned the 166 out of 286 areas a label of "Gordon Subset" and repeated the analysis above 1000 times to obtain a null distribution.

2.8. Moving Average Analysis Across Age

To examine the FC fit to different network schemes across infancy, we used a moving average analysis across age. For this analysis, we limited our data to the 281 sessions collected at the age of 8-27 months because the data became very sparse and less evenly distributed after 27 months (Supplementary Figure 1). We first sorted the fMRI sessions by age at scan. Sessions were arranged chronologically by age, and FC averages were computed for consecutive windows of 20 sessions, with each window representing the mean age within it. This window was then shifted by one session at a time until all 281 sessions were accounted for. Subsequently, we calculated the average similarity index (SI) using the same method.

2.9. Age effect of within-network FC

To test the hypothesis that the subset of areas has relatively stable within-network FC across chronological age in infants, we compared the age effect on within-

network FC when the networks include only the subset versus full set of areas. The age effect of within-network FC was quantified with a Spearman's correlation (ρ). The significance of the difference between the correlation between chronological age and within-network FC in the subset versus full set of areas is calculated with a Z-test on Fisher-Z-transformed r values.

2.10. Intraclass Correlation Coefficient

To assess the differences in reliability of within-network edges for using the Gordon networks with all areas versus the subset of areas. We quantified the test-retest reliability of FC with intraclass correlation coefficient (ICC). We assessed the consistency among measurements under the fixed levels of the session factor (Tozzi et al., 2020), referred to as ICC 'C-1' (McGraw & Wong, 1996) or ICC (3,1) (Shrout & Fleiss, 1979).

For this analysis, we re-calculated the FC matrices for each individual with two non-overlapping time windows of data from each session. "Test" and "re-test" were defined as the first 6 min and last 6 min of low-motion data, separated by at least 1.2 min low motion data in between to reduce the impact of temporal autocorrelation (i.e. total > 13.2 min low-motion data). Only 167 sessions had enough low-motion data for this analysis. First, the FC values in the upper triangle of each subject's connectivity matrix were entered as rows in two large matrices (one matrix for "test" and another for "re-test", one row per subject in each matrix). Then, the corresponding columns of these matrices were compared to obtain an ICC value for each edge. The mean and standard error of the mean of the ICCs within each of the Gordon networks were calculated for the full and subset of the areas.

2.11. Group consistency and differential power of FC edges

Prior studies suggested that it was possible to identify individuals using FC in infants from the BCP dataset (Hu et al., 2022; Kardan et al., 2022). To assess which FC edges (i.e. connections between a pair of areas) are more consistent across individuals versus distinct across individuals, we calculated the group consistency (ϕ) and differential power (DP) measures (Finn et al., 2015). We aim to describe the distribution of highly consistent edges and highly differentiating edges with respect to adult and infant network models. For this analysis, we only use the one session from each of the 115 unique subjects with at least 13.2 min low-motion data. Given two sets of connectivity [X_i^{R1}], [X_i^{R2}] obtained from the two resting scan windows (*R1* and *R2*) after z-score normalization, the edgewise product vector φ_i was computed as

$$\varphi_i\,(e) = X_i^{R1}(e) * X_i^{R2}(e), e = 1, \dots, M \;(Equation\ 2)$$

where *i* indexed the subject, *e* indexed the edge, and *M* indexed the total number of FC edges. The sum of φ_i over all edges is the correlation between [X_i^{R1}], [X_i^{R2}]. The group consistency ϕ was computed as the mean of φ_i across all subjects. We defined the edges with the top 10% ϕ values to be "highly consistent".

Similarly, the edgewise product vector φ_{ij} was calculated between patterns from different subjects, for example:

$$\varphi_{ij}\,(e) = X_i^{R1}(e) * X_j^{R2}(e), e = 1, \dots, M, i \neq j \;(Equation\ 3)$$

$$P_i(e) = P\left|\varphi_{ij}(e) > \varphi_{ii}(e) \; or \; \varphi_{ji}(e) > \varphi_{ii}(e)\right| \; (Equation\ 4)$$

$$DP(e) = \sum_i \{-\ln(P_i(e))\} \; (Equation\ 5)$$

We defined the edges with the top 10% DP values as “highly differentiating”.

3. Results (currently 1643 words)

3.1. Adult and Infant functional connectivity clustering were best described by the adult and infant network assignments respectively

Gordon networks (adult) (Figure 1A) and Kardan networks (infant) (Figure 1B) assignments demonstrate a reasonable degree of agreement: Normalized Mutual Information (NMI) = 0.5 for the overlapping 281 areas after excluding the “None”/ “Unspecified” network in both adult and infant network assignments. The CON, pDMN, aDMN, SMN, mVis and lVis networks in the Kardan networks tend to have a large dice overlap with a single Gordon network, but Tem, DAN, pFPN, aFPN have a match to multiple Gordon networks (Supplementary Figure 2).

Next, we asked how closely the network assignments matched the similarity of FC profiles within and between different networks and quantified it with the silhouette index (SI; Rousseeuw, 1987; Yeo et al., 2011). We used the average FC across 120 adult sessions and the average FC across 313 infant sessions. We found that adult FC had a more modular organization (Figure 1C) when grouping into adult networks (Figure 1A) than infant networks (Figure 1E). The average SI for areas assigned to adult networks in adult FC (0.333, 95% bootstrap CI = [0.3088, 0.3417]) was much higher than the average SI for areas assigned to infant networks in adult FC (0.009, 95% bootstrap CI = [-0.0015, 0.0168]). In contrast, the opposite was observed for infant FC, with a higher average SI for areas assigned to infant networks in infant FC (0.336, 95% bootstrap CI = [0.3280, 0.3397], Figure 1F) than the average SI for areas assigned to adult networks in infant FC (0.049, 95% bootstrap CI = [0.0406,0.0560], Figure 1D). Furthermore, the results were also qualitatively validated across individual sessions, with a much higher SI of adult networks than infant networks on adult FC (Cohen’s d = 1.215, $p < 0.001$) (Supplementary Figure 3C), and a much higher SI of infant networks than adult networks on infant FC (Cohen’s d = 2.744, $p < 0.001$) (Supplementary Figure 4C). Taken together, the adult networks better describe the modular organization in adult FC than infant FC, and the infant networks better describe the modular organization in infant FC than adult FC. However, the SI is comparable for adult FC and infant FC using the best network model, suggesting the presence of the modular organization in both cohorts.

Notably, some areas tend to have a positive SI for areas assigned to adult networks regardless of the FC age group (Figure 1G & I). Since the spatial distribution of SI across sessions (Supplementary 3A-B & 4A-B) was relatively consistent, it is unlikely that the low SI magnitude in infants was purely driven by high interindividual variability.

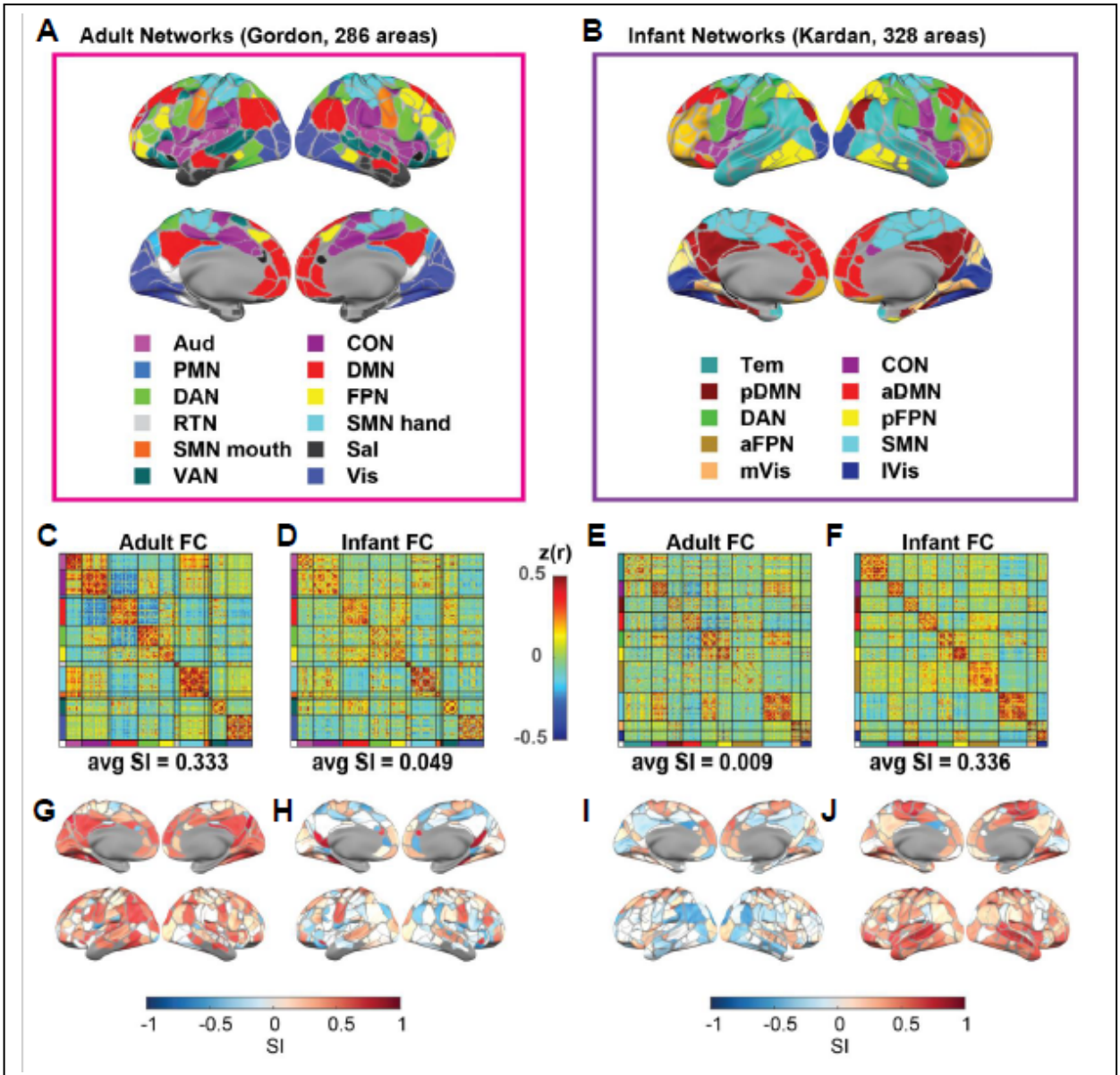

Figure 1. *Adult and Infant functional connectivity ordered by the adult and infant networks.* A) 12 adult networks, B) 10 infant networks, C) average adult FC sorted by adult networks, D) average infant FC sorted by adult networks, E) average adult FC sorted by infant networks, F) average infant FC sorted by infant networks, G) SI of parcels with adult network assignments in adults, H) SI of parcels with adult network assignments in infants, I) SI of parcels with infant network assignments in adults, J) SI of parcels with infant network assignments in infants. Network abbreviations: auditory (Aud), cingulo-opercular (CON), parietal memory (PMN), default mode (DMN), dorsal attention (DAN), fronto-parietal (FPN), retrosplenial temporal (RTN), somatomotor hand (SMN hand), somatomotor mouth (SMN mouth), salience (Sal), and ventral attention (VAN), visual (Vis), somatomotor (SMN), temporal (Tem), posterior frontoparietal (pFPN), posterior default mode (pDMN), lateral visual (lVis), medial visual (mVis), anterior fronto-parietal (aFPN), anterior default mode (aDMN).

3.2. A subset of areas demonstrates adult-like network organization throughout development

An SI above zero for an area indicates that its FC profile more closely resembles those of other areas in the same network than those in any alternative network within a given network scheme (e.g., adult Gordon networks). Therefore, we selected the subset of areas with an SI above zero when the adult networks were applied to the infant FC (166 areas in total, Figure 2A). These areas fell into all 11 out of the 12 Gordon networks (i.e., all except for PMN), with the whole RTN, SMN mouth and Sal networks retained, and the remaining 8 networks partially retained (Figure 2B). We validated that the areas with SI above zero are highly consistent across bootstrap samples, with 156 out of the 166 areas having SI above zero in at least 950 out of 1000 bootstraps (Supplementary Figure 6).

As expected, the average SI for areas assigned to adult networks in infant FC was much higher using the subset of areas than all areas (0.388, 95% bootstrap CI = [0.3792, 0.3925]; Figure 2C). The average SI for areas assigned to adult networks in adult FC was also marginally higher using the subset (0.419, 95% bootstrap CI = [0.3925,0.4300]) (Supplementary Figure 7A), suggesting that this subset captured the areas that are most coherently organized into the adult networks in both infants and adults. Compared to "Gordon Full" (286 areas, Figure 1A), "Gordon Subset" was disproportionally enriched in the SMN networks (SMN hand and SMN mouth) (Figure 2D). As expected, the within-network FC was significantly higher across infant sessions (paired t-test, FDR-corrected $p < 0.05$) for all 8 partially retained networks compared to full networks, with little change in variability (Figure 2E). Similarly, the within-network FC was significantly higher across adult sessions (paired t-test, FDR-corrected $p < 0.05$) for all seven out of eight partially retained networks, and significantly lower across adult sessions for FPN. In general, the within-network FC differences between "Gordon Full" and "Gordon Subset" were larger in infants than in adults (Table 1).

Table 1. *Cohen's d of the within-network FC differences in Gordon Full V.S. Gordon Subset.*

	Aud	CON	DMN	DAN	FPN	SMN hand	VAN	Vis
Infant FC	-2.41	-0.29	-1.80	-2.23	-1.54	-2.81	-2.64	-2.91
Adult FC	-1.13	-0.31	-0.46	-1.47	0.70	-1.09	-1.53	-2.10

It was implied from the results above that the difference in within-network FC between adults and infants would be smaller when using the "Gordon Subset" compared to the "Gordon Full". We tested this directly using a two-sample t-test (Figure 3, Table 2). We found that in seven out of the eight partially retained Gordon networks the adult FC was significantly higher (FDR-corrected $p < 0.05$) than the infant FC with the "Gordon Full" area set (Figure 3A). On the other hand, only five out of the eight still demonstrated significantly higher within-network FC (FDR-corrected $p < 0.05$) in adults compared to infants, and two out of the eight demonstrated significantly lower within-network FC (FDR-corrected $p < 0.05$) (Figure 3B).

Table 2. *Cohen's d of the within-network FC differences in adults V.S. infants*

	Aud	CON	DMN	DAN	FPN	SMN hand	VAN	Vis
Gordon Full	2.35	2.35	0.80	2.11	0.23	1.04	0.03	1.22
Gordon Subset	1.04	1.88	0.13	1.04	-0.26	0.43	-0.34	0.94

Additionally, we found that the effect of chronological age on within-network FC within the infant cohort was also reduced when the "Gordon Subset" was used in place of "Gordon Full" (Supplementary Figure 8). The details are reported in the Supplementary Materials.

Taken together, this suggested that while the within-network FC within "Subset" was higher than within "Full" in both infant and adult datasets, using the "Subset" compared to "Full" reduced the difference across age.

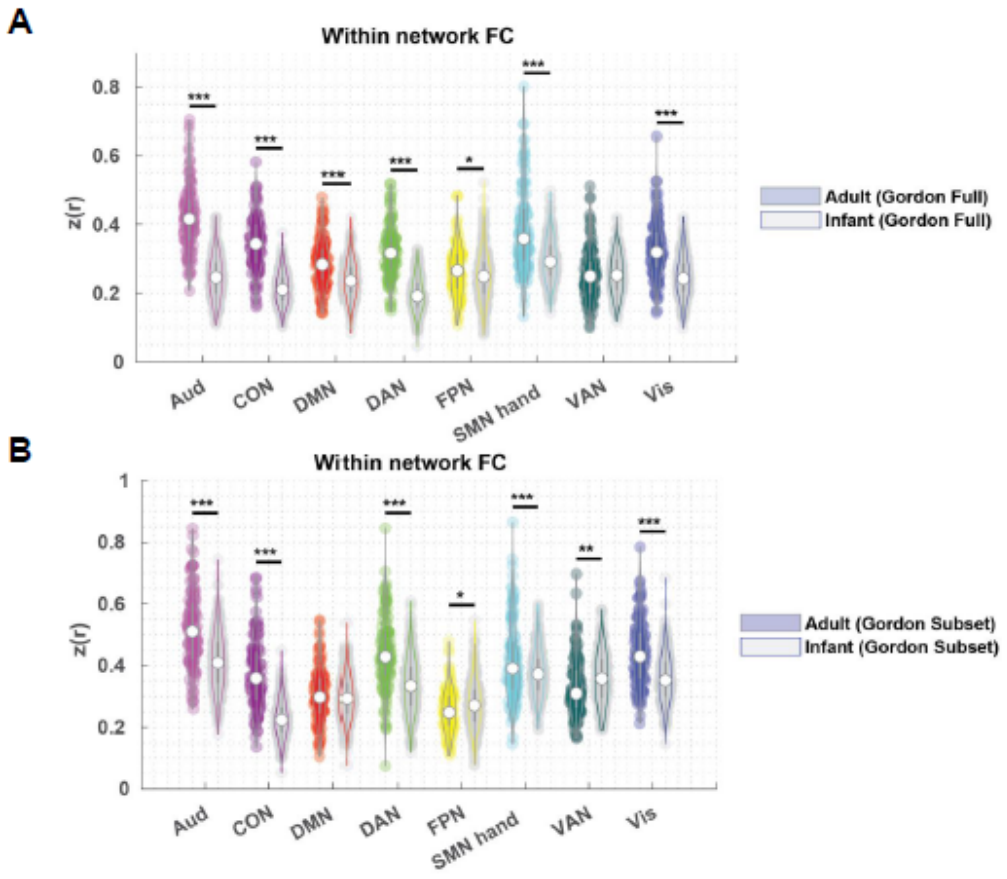

Figure 3. *Violin plot of within-network average FC in the Gordon networks.* A) within-network average FC using the full sets of areas in adults and infants. B) Within-network average FC using the subset of areas in adults and infants. FDR-corrected p for two-sample t-tests. * $p < 0.05$, ** $p < 0.01$, *** $p < 0.001$.

3.4. Adult versus infant network across 1-2-year-olds

Next, we asked whether there was any variation between how the different network schemes fit the infant FC at various stages between 1 to 2 years (Gordon adult networks and Kardan infant networks). In addition, we also applied the Gordon and Kardan network sorting on the subset of 166 areas in Figure 2A. Using a moving average approach across infant ages, we found a consistent order of the network schemes, with the Gordon (Subset), Kardan and Kardan (Subset) having a similar average SI, and Gordon networks having a much lower average SI (Figure 4A). When comparing 1 year (Figure 4B) and 2 years (Figure 4C). We found a marginal increase in the average SI for the Gordon networks, even though the 95% bootstrap confidence

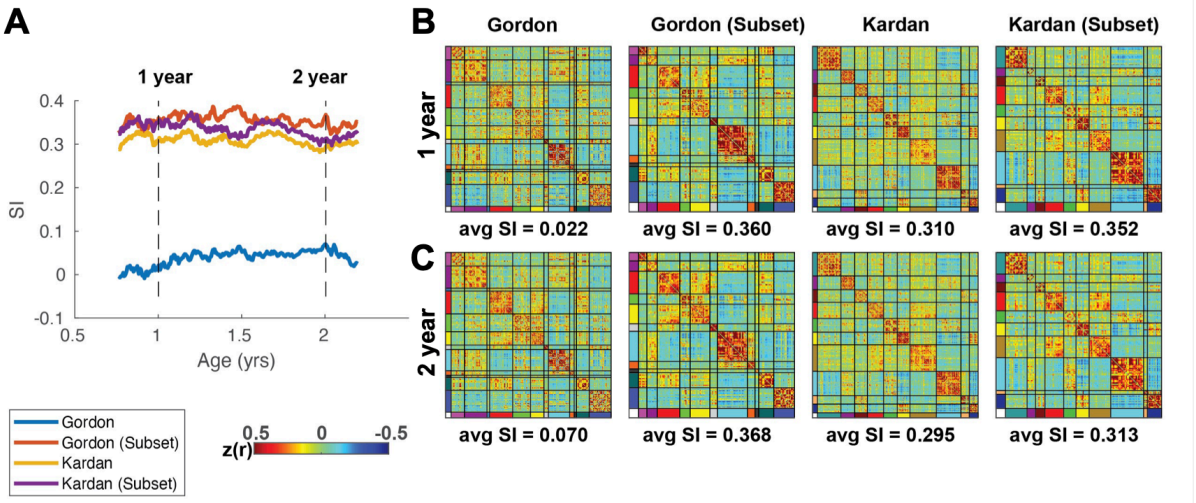

Figure 4. *Moving average analysis with the adult networks, the subset of the adult networks, and the infant networks.* A) Average SI of the average FC in a window for different network assignments. B) Average SI of the window around 1 year old sorted by different network assignments. C) Average SI of the window around 2 years old sorted by different network assignments.

interval across 1000 bootstraps did not overlap (Supplementary Figure 9).

3.5. The subset of areas with adult-like network organization is in spatial proximity to the high consensus regions across adult individuals

To quantify the spatial distribution similarity between the locations of low interindividual variability in network identity ("high consensus cortical ROIs") (Dworetsky et al., 2021) and the "Gordon Subset" areas, we calculated the Euclidean distance between the centers of the "Gordon Subset" areas (Figure 5A) and the alternative "not Gordon Subset" areas (Figure 5B) by 3.9 mm (~1 voxel). To rule out the possibility that this difference was driven by the differences in the number of areas, we repeated the same analysis by permuting "Gordon Subset" (N = 166) versus "not Gordon Subset" (N = 120) labels 1000 times to generate a null distribution. We found that the actual difference (3.9 mm) was significantly higher than the null ($p < 0.001$, permutation testing) (Figure 5C).

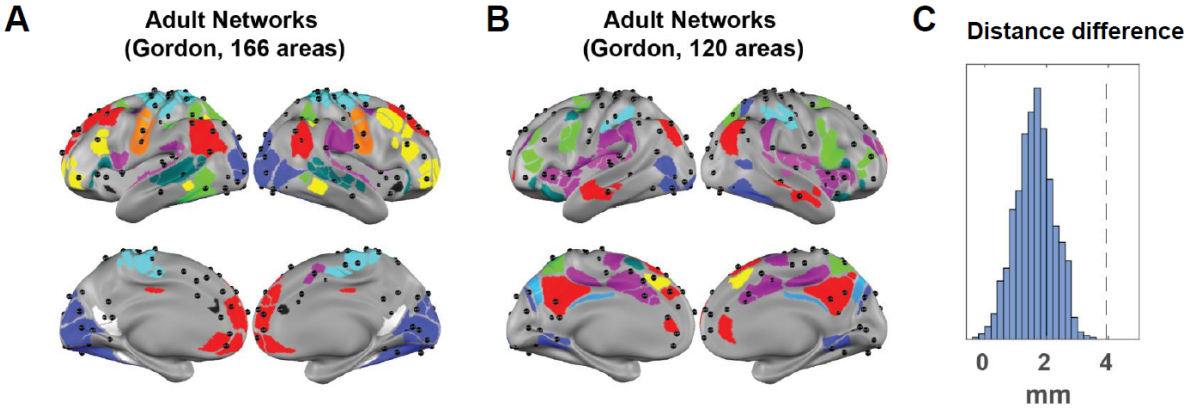

Figure 5. *Compare the subset of parcels with adult-like network organization to high-consensus regions.* A) The subset of parcels with adult-like network organization overlayed with high-consensus regions. B) The remaining parcels overlayed with high-consensus regions. C) The average Euclidean distance between the high-consensus regions and the closest parcel center. Dashed line: the actual difference between the distances in panel A and panel B. Histogram: the difference between the distances with parcels randomly assigned to be in the adult-like (panel A) and not adult-like (panel B) groups 1000 times.

3.6. Within-network FC edges in the subset of areas has a higher test-retest reliability and a higher consistency across subjects

Comparing FC computed from non-overlapping time windows in the same session demonstrated that the subset parcels had significantly higher within-session reliability than the full parcel set. In particular, the four out of eight networks with partially retained parcels exhibited higher average ICC with the parcel subset than the full parcel set (two-sample t-test, FDR-corrected $p < 0.05$): Aud (Cohen's $d = 0.68$), DMN (Cohen's $d = 0.13$), DAN (Cohen's $d = 0.55$), and VAN (Cohen's $d = 0.43$) (Figure 6)

To examine whether the contribution of FC edges to individual identification varied across the within- and between-network blocks by the three network schemes, we also quantified the FC group consistency (ϕ) and differential power (DP) (Finn et al., 2015). Consistent with previous literature, we observed that a large percentage (~50%) of FC edges in the within-network blocks tend to be highly consistent in all three network schemes, as opposed to between-network blocks (~6%) (Supplementary Figure 10; Supplementary Table 1). The sensorimotor networks especially had a large proportion of highly consistent within-network FC edges (Supplementary Table 1-2). Moreover, using adult networks defined by the subset of areas ("Gordon Subset"), the percentage of high consistent edges within network increased dramatically for all eight partially retained networks (Supplementary Table 2), suggesting that the adult network spanned by our subset over-represented areas with highly consistent FC between them.

On the other hand, within-network blocks tend to have only a slightly larger percentage of highly differentiating FC edges (~15%) than between-network blocks (~10%) (Supplementary Table 3), with both increased and decreased proportion of highly differentiating edges when using the "Gordon Subset" instead of "Gordon Full".

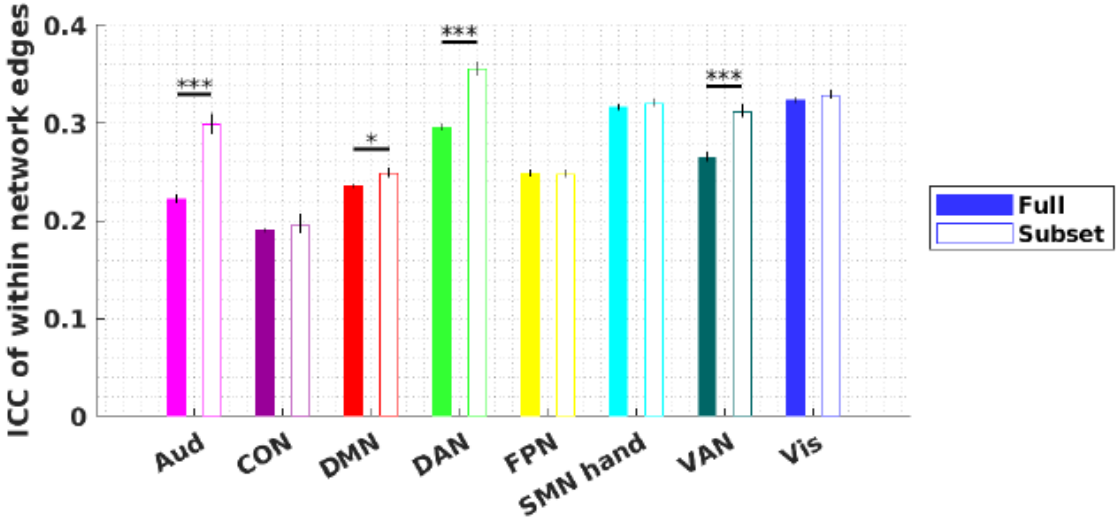

Figure 6. *Reliability of within-network edges using the full versus subset of parcels.* Reliability of within-network edges across two non-overlapping 6-minute windows. Bars show the mean of the ICC and error bars show the standard error of the mean. * $p < 0.05$, ** $p < 0.01$, *** $p < 0.001$. p-values are FDR-corrected following two-sample t-tests.

4. Discussion

4.1. Infant FC has a modular structure distinct from adult FC

We observed that for infants at 8-60 months, brain areas did exhibit some degree of clustering in average FC profiles according to the adult network assignments (average SI>0), although much weaker than that in adult FC. This observation is consistent with prior literature where a modular organization of FC was detected in preterm-born (Cao et al., 2017; van den Heuvel et al., 2015) and *in utero* fetal baby brains (Thomason et al., 2014; Wheelock et al., 2019), with a decent degree of similarity to the modular organization in the adult FC (van den Heuvel et al., 2015). Furthermore, it seemed that instead of being less modular and more random, the infant FC data were better described with notably different but related modular organization, including fragmented anterior and posterior segments of higher-order association networks (Eggebrecht et al., 2017; Eyre et al., 2021; Kardan et al., 2022; Marrus et al., 2018).

4.2. Identification of functional network cores that are stable across development

We found that a subset of the areas tended to exhibit more of an adult-like network FC clustering pattern, forming the “network cores” of adult networks. While the unique and evolving modular organization in infant FC has been an interesting and important topic of study (F. Wang et al., 2023; Wen et al., 2019, 2020), it is also desirable to note their similarities to older children and adults (Fransson et al., 2007; Gao, Alcauter, Elton, et al., 2015). The difference in within-network FC across ages was reduced when this subset was used instead of the full set of brain areas. The FC within this subset of regions was also more consistent across sessions and individuals. These areas likely form the early scaffold for what will eventually become the adult networks (Grayson & Fair, 2017).

4.3. The role of childhood experience in shaping the development of functional networks

Our results hinted that interindividual variability in functional network topography might have a developmental origin. To a first approximation, the spatial topography of the network cores we found resembled that of the locations with low interindividual variability in network identity (Dworetsky et al., 2021; Gordon, Laumann, Gilmore, et al., 2017; Hermosillo et al., 2024), while the areas that are subject to misidentification in infants resembled integration zones with a high degree of network overlap (Hermosillo et al., 2024) and network hubs with a high participation coefficient (Power et al., 2013).

One potential explanation for this observation is that some parts of the brain matured *in utero* and, thus, showed limited plasticity after birth, while other parts continue to develop throughout childhood. In line with this, mature synaptic density, cortical thickness, and gray matter density were reached earlier in low-expanding regions (e.g. V1 and Heschl's gyrus) than in high-expanding regions (DLPFC) (Hill et al., 2010). There might be biological or evolutionary reasons to have parts of the adult networks maturing later, such as to limit the prenatal resources on regions most important for early survival and increase the influence of postnatal experience on other regions (Hill et al., 2010). In addition, the regional variability of network stability might also be linked to variability in the expression of excitatory and inhibitory features across the cortex (Sydnor et al., 2021). The idea that areas with higher FC variability had more behavioral significance is further reinforced by research demonstrating that behavioral and cognitive domain features could be better predicted from FC in cortical areas with high FC variability (Mueller et al., 2013). Recognition of the regional variability in functional network stability across development in future research is important, as they may become useful biomarkers for psychopathology (Sydnor et al., 2021), as well as therapeutic targets for brain stimulation interventions (Correll et al., 2021).

We did not observe a strong over-representation of sensorimotor networks compared to association networks in our stable network cores, despite the literature suggesting that sensorimotor networks mature early than association networks (Gao, Alcauter, Elton, et al., 2015; Sydnor et al., 2021). The network cores spanned both sensorimotor and association networks along the functional hierarchy of the neocortex (Flechsig, 1901; Mesulam, 1998; Sydnor et al., 2021). One potential limitation is that our infant cohort was older than eight months and significant earlier neurodevelopmental changes along the sensorimotor-association hierarchy might have happened before eight months (Bethlehem et al., 2022; Flechsig, 1901). Another possibility is that the sensorimotor functional networks definition was inaccurate, e.g. the auditory network might incorporated parts of secondary somatosensory regions (Raju & Tadi, 2024), making the areas within the network less similar in their FC profile.

4.4. Using a subset of areas to improve statistical power and interpretability

There are pros and cons of using a pre-existing functional network model and a data-driven functional network model for infant neuroimaging research. Studies of functional networks in infants have often implemented unsupervised methods (i.e. clustering or similar types of community detection algorithms) to find age-specific modules and called them "functional networks" (Eggebrecht et al., 2017; Kardan et al., 2022; Marrus et al., 2018; Molloy & Saygin, 2022; Myers et al., 2024; Sylvester et al., 2022; F.

Wang et al., 2023; Wen et al., 2019, 2020). These identified modules were by definition a good representation of the organizational structure in the data and may help address the problem of reproducibility in brain-wise association studies (Hermosillo et al., 2024; Marek et al., 2022). However, unlike the adult networks that have been extensively validated with behavioral task data to corroborate their "functional" roles (Power et al., 2011; Wig, 2017; Yeo et al., 2011), those age-specific modules often lack biological support for their functions, making the relevance to a broader developmental context less obvious. On the other hand, using the adult-network topography directly on infants neglects the infant-specific organizational features and risks including spurious variability in measurements (be they from fMRI, EEG, or fNIRS), leading to reduced effect size and power (Hermosillo et al., 2024), or an exaggerated difference across development. For example, our results in section 3.2 suggested that differences in within-network FC across age groups might be partially attributed to the misspecification of functional network identity.

Here, we proposed an alternative strategy that used a subset of areas representing the stable "network cores" across infancy and adulthood for studying trajectories of FC during development. This approach strikes a balance between interpretability/comparability across cohorts, and reliability/reproducibility. This idea of using a subset of the brain areas to define ROIs as an approach to improve statistical power has been proposed in the literature (Dworetsky et al., 2021; Hermosillo et al., 2024). However, instead of focusing the subset of brain areas with interindividual variability, we focused on excluding the subset of brain areas that had a network misidentification in the infant cohort. Alternatively, depending on the research question at hand, one might be interested in focusing on the areas that are unstable across development, which may have behavioral or clinical significance as mentioned in section 4.3.

4.5. Precision Functional Mapping in Developmental Cohorts Using Adult Group Priors Needs to Be Practiced with Caution

As demonstrated in our results, on average the adult functional networks did not well represent the organization of infant FC into internally similar clusters, which might have important implications for research using an adult functional network model to generate individual-specific functional networks in the developmental cohort. Recent research has recognized idiosyncratic details and reliable features in functional network topography across human individuals qualitatively different from group-average estimates (Gordon et al., 2015; Gordon, Laumann, Gilmore, et al., 2017; Gratton et al., 2018; Laumann et al., 2015). Those features are stable across sessions (Seitzman et al., 2019), as well as task versus rest states (Kraus et al., 2021). The individual differences in association network topography also predict individual differences in executive function (Cui et al., 2020). However, reliable identification of individualized functional networks with unsupervised clustering or community detection procedures requires extended data acquisition. For example, with the Infomap algorithm (Power et al., 2011; Rosvall & Bergstrom, 2008), more than 90 minutes of data is required to achieve an average network overlap dice coefficient of > 0.75 (Gordon, Laumann, Gilmore, et al., 2017). Therefore, several semi-supervised methods have been developed to derive individual functional networks (Cui et al., 2020; Gordon, Laumann, Adeyemo, et al., 2017; Hacker et al., 2013; Kong et al., 2019; D. Wang et al., 2015) using adult networks as priors.

716 However, those approaches generally assumed that the individual functional networks
717 were highly similar to the adult group average. This assumption might not be suitable for
718 developmental cohorts: as we demonstrated here, on average, the adult functional
719 networks poorly represented the organization of the infant FC into internally coherent
720 clusters. Two unwanted consequences might arise from this observation. First, the
721 network templates generated by averaging the FC profiles within a poorly defined network
722 might be noisy and inaccurate. Second, the algorithms may incorrectly force a categorical
723 label for locations that poorly matched all available networks. Future studies using adult-
724 based priors in developmental cohorts should keep those limitations in mind and develop
725 strategies to mitigate them.
726
727 **4.6. Limitations and Future Directions**
728 Our infant fMRI data were collected during natural sleep while adult networks were
729 derived from awake resting state data. Since sleep and the level of arousal are known to
730 modify the FC structure in adults (Chang et al., 2016; Mitra et al., 2017; Tagliazucchi et
731 al., 2012), and that FC patterns in asleep 6 and 12 months old infants more closely
732 resemble FC patterns in asleep adults (Mitra et al., 2017), the difference in modularity
733 and hence in the quality of clustering as measured by the silhouette index between adult
734 and infant FC using the adult Gordon network might be smaller if the infant fMRI data
735 were collected during an awake state. Other differences in the acquisition and processing
736 of the two datasets might introduce confounds, too. Additionally, while we observed little
737 age effect on within-network FC, this could be due to the narrow age range of our sample
738 (mostly between 1 and 3 years). Moreover, we used an adult area parcellation (Gordon
739 et al., 2016) for the adult (Gordon et al., 2016) and infant (Kardan et al., 2022), which was
740 slightly inferior to an age-specific parcellation for the toddler group to describe the local
741 area organization at this age based on our preliminary analysis. The mixing of fMRI
742 signals within the ill-defined areas might contributed to some of the low SI observed in
743 those areas. In the future, the same analysis strategy could be applied directly to
744 vertex/voxel level data for higher precision.
745 Future studies could examine the cellular, molecular, and genetic properties of the
746 areas that have already developed an adult-like organization in infancy to fully understand
747 the biological underpinning of our observation. Furthermore, given that we expect that
748 using the subset of areas that form relatively stable network organization across
749 development would improve statistical power for brain-wide association studies (Marek
750 et al., 2022) using FC, future studies with larger samples and well-defined behavior
751 measures with reliability tests used in prior literature can be used to test this hypothesis
752 (Hermosillo et al., 2024; Marek et al., 2022). Moreover, it would be interesting to
753 investigate whether the same “network cores” exist in subcortical structures, such as the
754 thalamus. One plausible hypothesis is that the topography and diversity of thalamocortical
755 projection may relate to the variability of functional network stability across the neocortex.
756
757 **4.7. Conclusion**
758 We found that despite the large differences in FC organization between infants
759 and adults on average, there existed a subset of cortical areas whose FC profiles
760 demonstrated adult-like network organization even in infants. These areas were spatially
761 closer to previously locations of high consensus in network identity across adult

individuals than alternative areas. Additionally, within-network FC defined with the subset of areas was higher in magnitude and more reliable across scans, individuals, and development. We proposed the use of adult networks defined by the subset of areas with an adult-like network relationship as a complementary approach of studying infant FC than using age-specific functional networks derived from data-driven methods. This would strengthen reliability, yet at the same time encourage interpretability and comparability across developmental stages. The biological basis of the regional variability of functional network stability, as well as its psychopathological and behavioral impacts may become interesting topics for future research.

Author Contributions

JCT conceptualized the project. JCT and YW conducted a formal analysis. OK, OM, TKMD, CMS, DD, XW, and YW processed/curated the data. MDW, JCT, JTE were responsible for funding acquisition. JCT and MDW wrote the original draft. Everyone contributed to the review and editing of the final manuscript.

Funding

This work is partially supported by the CCSN fellowship from the McDonnell Center for Systems Neuroscience at Washington University School of Medicine in St. Louis to JCT and from NIH grants including EB029343 to MDW. The Baby Connectome Project was supported by NIMH R01 MH104324 and NIMH U01 MH110274.

Declaration of Competing Interests

The authors declared that they have no competing financial interests or personal relationships that could have appeared to influence the work reported in this paper.

Data and Code Availability

The WU 120 data can be downloaded from https://legacy.openfmri.org/dataset/ds000243/.

The BCP data can be downloaded from the National Institute of Mental Health Data Archive (NDA) at https://nda.nih.gov/edit_collection.html?id= 2848. The preprocessing scripts are available at https:// github.com/DCAN-Labs/dcan-infant-pipeline. The analysis scripts used to generate the results and figures are available on https://github.com/cindyhfls/Tu-2024-GordonSubset-DCN.

The test for the difference between correlations were implemented from the function corr_rtest downloaded from MATLAB central. The Intraclass Correlation Coefficient (ICC) was calculated from the function ICC downloaded from MATLAB central.

Acknowledgement

The authors would like to thank Ari Segel for assistance in statistical analysis. The authors would also like to thank all families participated and technicians who have helped with the collection, processing, and curation of the data.

Declaration of generative AI and AI-assisted technologies in the writing process

During the preparation of this work the authors used ChatGPT in order to improve sentence structure and language precision. After using this tool/service, the authors reviewed and edited the content as needed and take full responsibility for the content of the publication.

References

Ahmad, S., Wu, Y., Wu, Z., Thung, K.-H., Liu, S., Lin, W., Li, G., Wang, L., & Yap, P.-T. (2023). Multifaceted atlases of the human brain in its infancy. *Nature Methods*, *20*(1), Article 1. https://doi.org/10.1038/s41592-022-01703-z

Bethlehem, R. a. I., Seidlitz, J., White, S. R., Vogel, J. W., Anderson, K. M., Adamson, C., Adler, S., Alexopoulos, G. S., Anagnostou, E., Areces-Gonzalez, A., Astle, D. E., Auyeung, B., Ayub, M., Bae, J., Ball, G., Baron-Cohen, S., Beare, R., Bedford, S. A., Benegal, V., … Alexander-Bloch, A. F. (2022). Brain charts for the human lifespan. *Nature*, *604*(7906), Article 7906. https://doi.org/10.1038/s41586-022-04554-y

Bijsterbosch, J. D., Beckmann, C. F., Woolrich, M. W., Smith, S. M., & Harrison, S. J. (2019). The relationship between spatial configuration and functional connectivity of brain regions revisited. *eLife*, *8*, e44890. https://doi.org/10.7554/eLife.44890

Bijsterbosch, J. D., Woolrich, M. W., Glasser, M. F., Robinson, E. C., Beckmann, C. F., Van Essen, D. C., Harrison, S. J., & Smith, S. M. (2018). The relationship between spatial configuration and functional connectivity of brain regions. *eLife*, *7*, e32992. https://doi.org/10.7554/eLife.32992

Cao, M., He, Y., Dai, Z., Liao, X., Jeon, T., Ouyang, M., Chalak, L., Bi, Y., Rollins, N., Dong, Q., & Huang, H. (2017). Early Development of Functional Network Segregation Revealed by Connectomic Analysis of the Preterm Human Brain. *Cerebral Cortex*, *27*(3), 1949–1963. https://doi.org/10.1093/cercor/bhw038

Chang, C., Leopold, D. A., Schölvinck, M. L., Mandelkow, H., Picchioni, D., Liu, X., Ye, F. Q., Turchi, J. N., & Duyn, J. H. (2016). Tracking brain arousal fluctuations with fMRI. *Proceedings of the National Academy of Sciences*, *113*(16), 4518–4523. https://doi.org/10.1073/pnas.1520613113

Correll, C. U., Cortese, S., Croatto, G., Monaco, F., Krinitski, D., Arrondo, G., Ostinelli, E. G., Zangani, C., Fornaro, M., Estradé, A., Fusar-Poli, P., Carvalho, A. F., & Solmi, M. (2021). Efficacy and acceptability of pharmacological, psychosocial, and brain stimulation interventions in children and adolescents with mental disorders: An umbrella review. *World Psychiatry*, *20*(2), 244–275. https://doi.org/10.1002/wps.20881

Cui, Z., Li, H., Xia, C. H., Larsen, B., Adebimpe, A., Baum, G. L., Cieslak, M., Gur, R. E., Gur, R. C., Moore, T. M., Oathes, D. J., Alexander-Bloch, A. F., Raznahan, A., Roalf, D. R., Shinohara, R. T., Wolf, D. H., Davatzikos, C., Bassett, D. S., Fair, D. A., … Satterthwaite, T. D. (2020). Individual Variation in Functional Topography of Association Networks in Youth. *Neuron*, *106*(2), 340-353.e8. https://doi.org/10.1016/j.neuron.2020.01.029

Dworetsky, A., Seitzman, B. A., Adeyemo, B., Neta, M., Coalson, R. S., Petersen, S. E., & Gratton, C. (2021). Probabilistic mapping of human functional brain networks identifies regions of

high group consensus. *NeuroImage*, *237*, 118164. https://doi.org/10.1016/j.neuroimage.2021.118164

Eggebrecht, A. T., Elison, J. T., Feczko, E., Todorov, A., Wolff, J. J., Kandala, S., Adams, C. M., Snyder, A. Z., Lewis, J. D., Estes, A. M., Zwaigenbaum, L., Botteron, K. N., McKinstry, R. C., Constantino, J. N., Evans, A., Hazlett, H. C., Dager, S., Paterson, S. J., Schultz, R. T., … Pruett, J. R., Jr. (2017). Joint Attention and Brain Functional Connectivity in Infants and Toddlers. *Cerebral Cortex*, *27*(3), 1709–1720. https://doi.org/10.1093/cercor/bhw403

Eyre, M., Fitzgibbon, S. P., Ciarrusta, J., Cordero-Grande, L., Price, A. N., Poppe, T., Schuh, A., Hughes, E., O'Keeffe, C., Brandon, J., Cromb, D., Vecchiato, K., Andersson, J., Duff, E. P., Counsell, S. J., Smith, S. M., Rueckert, D., Hajnal, J. V., Arichi, T., … Edwards, A. D. (2021). The Developing Human Connectome Project: Typical and disrupted perinatal functional connectivity. *Brain*, *144*(7), 2199–2213. https://doi.org/10.1093/brain/awab118

Fair, D. A. (2020). Correction of respiratory artifacts in MRI head motion estimates. *NeuroImage*, 17.

Feczko, E., Conan, G., Marek, S., Tervo-Clemmens, B., Cordova, M., Doyle, O., Earl, E., Perrone, A., Sturgeon, D., Klein, R., Harman, G., Kilamovich, D., Hermosillo, R., Miranda-Dominguez, O., Adebimpe, A., Bertolero, M., Cieslak, M., Covitz, S., Hendrickson, T., … Fair, D. A. (2021). *Adolescent Brain Cognitive Development (ABCD) Community MRI Collection and Utilities* (p. 2021.07.09.451638). bioRxiv. https://doi.org/10.1101/2021.07.09.451638

Finn, E. S., Shen, X., Scheinost, D., Rosenberg, M. D., Huang, J., Chun, M. M., Papademetris, X., & Constable, R. T. (2015). Functional connectome fingerprinting: Identifying individuals using patterns of brain connectivity. *Nature Neuroscience*, *18*(11), Article 11. https://doi.org/10.1038/nn.4135

Fischl, B. (2012). FreeSurfer. *NeuroImage*, *62*(2), 774–781. https://doi.org/10.1016/j.neuroimage.2012.01.021

Flechsig, P. (1901). DEVELOPMENTAL (MYELOGENETIC) LOCALISATION OF THE CEREBRAL CORTEX IN THE HUMAN SUBJECT. *The Lancet*, *158*(4077), 1027–1030. https://doi.org/10.1016/S0140-6736(01)01429-5

Fornito, A., Zalesky, A., & Breakspear, M. (2015). The connectomics of brain disorders. *Nature Reviews Neuroscience*, *16*(3), 159–172. https://doi.org/10.1038/nrn3901

Fox, M., & Greicius, M. (2010). Clinical applications of resting state functional connectivity. *Frontiers in Systems Neuroscience*, *4*. https://www.frontiersin.org/articles/10.3389/fnsys.2010.00019

Fransson, P., Skiöld, B., Horsch, S., Nordell, A., Blennow, M., Lagercrantz, H., & Åden, U. (2007). Resting-state networks in the infant brain. *Proceedings of the National Academy of Sciences*, *104*(39), 15531–15536. https://doi.org/10.1073/pnas.0704380104

Gao, W., Alcauter, S., Elton, A., Hernandez-Castillo, C. R., Smith, J. K., Ramirez, J., & Lin, W. (2015). Functional Network Development During the First Year: Relative Sequence and Socioeconomic Correlations. *Cerebral Cortex (New York, N.Y.: 1991)*, *25*(9), 2919–2928. https://doi.org/10.1093/cercor/bhu088

Gao, W., Alcauter, S., Smith, J. K., Gilmore, J. H., & Lin, W. (2015). Development of human brain cortical network architecture during infancy. *Brain Structure and Function*, *220*(2), 1173–1186. https://doi.org/10.1007/s00429-014-0710-3

Gao, W., Lin, W., Grewen, K., & Gilmore, J. H. (2017). Functional Connectivity of the Infant Human Brain: Plastic and Modifiable. *The Neuroscientist*, *23*(2), 169–184. https://doi.org/10.1177/1073858416635986

Gao, W., Zhu, H., Giovanello, K. S., Smith, J. K., Shen, D., Gilmore, J. H., & Lin, W. (2009). Evidence on the emergence of the brain's default network from 2-week-old to 2-year-old healthy pediatric subjects. *Proceedings of the National Academy of Sciences*, *106*(16), 6790–6795. https://doi.org/10.1073/pnas.0811221106

Garcia, K. E., Robinson, E. C., Alexopoulos, D., Dierker, D. L., Glasser, M. F., Coalson, T. S., Ortinau, C. M., Rueckert, D., Taber, L. A., Van Essen, D. C., Rogers, C. E., Smyser, C. D., & Bayly, P. V. (2018). Dynamic patterns of cortical expansion during folding of the preterm human brain. *Proceedings of the National Academy of Sciences of the United States of America*, *115*(12), 3156–3161. https://doi.org/10.1073/pnas.1715451115

Glasser, M. F., Sotiropoulos, S. N., Wilson, J. A., Coalson, T. S., Fischl, B., Andersson, J. L., Xu, J., Jbabdi, S., Webster, M., Polimeni, J. R., Van Essen, D. C., & Jenkinson, M. (2013). The minimal preprocessing pipelines for the Human Connectome Project. *NeuroImage*, *80*, 105–124. https://doi.org/10.1016/j.neuroimage.2013.04.127

Gordon, E. M., Laumann, T. O., Adeyemo, B., Huckins, J. F., Kelley, W. M., & Petersen, S. E. (2016). Generation and Evaluation of a Cortical Area Parcellation from Resting-State Correlations. *Cerebral Cortex*, *26*(1), 288–303. https://doi.org/10.1093/cercor/bhu239

Gordon, E. M., Laumann, T. O., Adeyemo, B., & Petersen, S. E. (2015). Individual Variability of the System-Level Organization of the Human Brain. *Cerebral Cortex*, bhv239. https://doi.org/10.1093/cercor/bhv239

Gordon, E. M., Laumann, T. O., Adeyemo, B., & Petersen, S. E. (2017). Individual Variability of the System-Level Organization of the Human Brain. *Cerebral Cortex*, *27*(1), 386–399. https://doi.org/10.1093/cercor/bhv239

Gordon, E. M., Laumann, T. O., Gilmore, A. W., Newbold, D. J., Greene, D. J., Berg, J. J., Ortega, M., Hoyt-Drazen, C., Gratton, C., Sun, H., Hampton, J. M., Coalson, R. S., Nguyen, A. L., McDermott, K. B., Shimony, J. S., Snyder, A. Z., Schlaggar, B. L., Petersen, S. E., Nelson, S. M., & Dosenbach, N. U. F. (2017). Precision Functional Mapping of Individual Human Brains. *Neuron*, *95*(4), 791-807.e7. https://doi.org/10.1016/j.neuron.2017.07.011

Gratton, C., Laumann, T. O., Nielsen, A. N., Greene, D. J., Gordon, E. M., Gilmore, A. W., Nelson, S. M., Coalson, R. S., Snyder, A. Z., Schlaggar, B. L., Dosenbach, N. U. F., & Petersen, S. E. (2018). Functional Brain Networks Are Dominated by Stable Group and Individual Factors, Not Cognitive or Daily Variation. *Neuron*, *98*(2), 439-452.e5. https://doi.org/10.1016/j.neuron.2018.03.035

Grayson, D. S., & Fair, D. A. (2017). Development of large-scale functional networks from birth to adulthood: A guide to the neuroimaging literature. *NeuroImage*, *160*, 15–31. https://doi.org/10.1016/j.neuroimage.2017.01.079

Hacker, C. D., Laumann, T. O., Szrama, N. P., Baldassarre, A., Snyder, A. Z., Leuthardt, E. C., & Corbetta, M. (2013). Resting state network estimation in individual subjects. *NeuroImage*, *82*, 616–633. https://doi.org/10.1016/j.neuroimage.2013.05.108

Hermosillo, R. J. M., Moore, L. A., Feczko, E., Miranda-Domínguez, Ó., Pines, A., Dworetsky, A., Conan, G., Mooney, M. A., Randolph, A., Graham, A., Adeyemo, B., Earl, E., Perrone, A., Carrasco, C. M., Uriarte-Lopez, J., Snider, K., Doyle, O., Cordova, M., Koirala, S., … Fair, D.

A. (2024). A precision functional atlas of personalized network topography and probabilities. *Nature Neuroscience*, *27*(5), 1000–1013. https://doi.org/10.1038/s41593-024-01596-5

Hill, J., Inder, T., Neil, J., Dierker, D., Harwell, J., & Van Essen, D. (2010). Similar patterns of cortical expansion during human development and evolution. *Proceedings of the National Academy of Sciences*, *107*(29), 13135–13140. https://doi.org/10.1073/pnas.1001229107

Howell, B. R., Styner, M. A., Gao, W., Yap, P.-T., Wang, L., Baluyot, K., Yacoub, E., Chen, G., Potts, T., Salzwedel, A., Li, G., Gilmore, J. H., Piven, J., Smith, J. K., Shen, D., Ugurbil, K., Zhu, H., Lin, W., & Elison, J. T. (2019). The UNC/UMN Baby Connectome Project (BCP): An overview of the study design and protocol development. *NeuroImage*, *185*, 891–905. https://doi.org/10.1016/j.neuroimage.2018.03.049

Hu, D., Wang, F., Zhang, H., Wu, Z., Zhou, Z., Li, G., Wang, L., Lin, W., Li, G., & Consortium, U. B. C. P. (2022). Existence of Functional Connectome Fingerprint during Infancy and Its Stability over Months. *Journal of Neuroscience*, *42*(3), 377–389. https://doi.org/10.1523/JNEUROSCI.0480-21.2021

Ji, J. L., Spronk, M., Kulkarni, K., Repovš, G., Anticevic, A., & Cole, M. W. (2019). Mapping the human brain's cortical-subcortical functional network organization. *NeuroImage*, *185*, 35–57. https://doi.org/10.1016/j.neuroimage.2018.10.006

Kaplan, S., Meyer, D., Miranda-Dominguez, O., Perrone, A., Earl, E., Alexopoulos, D., Barch, D. M., Day, T. K. M., Dust, J., Eggebrecht, A. T., Feczko, E., Kardan, O., Kenley, J. K., Rogers, C. E., Wheelock, M. D., Yacoub, E., Rosenberg, M., Elison, J. T., Fair, D. A., & Smyser, C. D. (2022). Filtering respiratory motion artifact from resting state fMRI data in infant and toddler populations. *NeuroImage*, *247*, 118838. https://doi.org/10.1016/j.neuroimage.2021.118838

Kardan, O., Kaplan, S., Wheelock, M. D., Feczko, E., Day, T. K. M., Miranda-Domínguez, Ó., Meyer, D., Eggebrecht, A. T., Moore, L. A., Sung, S., Chamberlain, T. A., Earl, E., Snider, K., Graham, A., Berman, M. G., Uğurbil, K., Yacoub, E., Elison, J. T., Smyser, C. D., … Rosenberg, M. D. (2022). Resting-state functional connectivity identifies individuals and predicts age in 8-to-26-month-olds. *Developmental Cognitive Neuroscience*, *56*, 101123. https://doi.org/10.1016/j.dcn.2022.101123

Kong, R., Li, J., Orban, C., Sabuncu, M. R., Liu, H., Schaefer, A., Sun, N., Zuo, X.-N., Holmes, A. J., Eickhoff, S. B., & Yeo, B. T. T. (2019). Spatial Topography of Individual-Specific Cortical Networks Predicts Human Cognition, Personality, and Emotion. *Cerebral Cortex*, *29*(6), 2533–2551. https://doi.org/10.1093/cercor/bhy123

Kraus, B. T., Perez, D., Ladwig, Z., Seitzman, B. A., Dworetsky, A., Petersen, S. E., & Gratton, C. (2021). Network variants are similar between task and rest states. *NeuroImage*, *229*, 117743. https://doi.org/10.1016/j.neuroimage.2021.117743

Lancaster, J. L., Glass, T. G., Lankipalli, B. R., Downs, H., Mayberg, H., & Fox, P. T. (1995). A modality-independent approach to spatial normalization of tomographic images of the human brain. *Human Brain Mapping*, *3*(3), 209–223. https://doi.org/10.1002/hbm.460030305

Langs, G., Wang, D., Golland, P., Mueller, S., Pan, R., Sabuncu, M. R., Sun, W., Li, K., & Liu, H. (2016). Identifying Shared Brain Networks in Individuals by Decoupling Functional and

Anatomical Variability. *Cerebral Cortex*, *26*(10), 4004–4014. https://doi.org/10.1093/cercor/bhv189

Laumann, T. O., Gordon, E. M., Adeyemo, B., Snyder, A. Z., Joo, S. J., Chen, M.-Y., Gilmore, A. W., McDermott, K. B., Nelson, S. M., Dosenbach, N. U. F., Schlaggar, B. L., Mumford, J. A., Poldrack, R. A., & Petersen, S. E. (2015). Functional System and Areal Organization of a Highly Sampled Individual Human Brain. *Neuron*, *87*(3), 657–670. https://doi.org/10.1016/j.neuron.2015.06.037

Marek, S., Tervo-Clemmens, B., Calabro, F. J., Montez, D. F., Kay, B. P., Hatoum, A. S., Donohue, M. R., Foran, W., Miller, R. L., Hendrickson, T. J., Malone, S. M., Kandala, S., Feczko, E., Miranda-Dominguez, O., Graham, A. M., Earl, E. A., Perrone, A. J., Cordova, M., Doyle, O., … Dosenbach, N. U. F. (2022). Reproducible brain-wide association studies require thousands of individuals. *Nature*, 1–7. https://doi.org/10.1038/s41586-022-04492-9

Marrus, N., Eggebrecht, A. T., Todorov, A., Elison, J. T., Wolff, J. J., Cole, L., Gao, W., Pandey, J., Shen, M. D., Swanson, M. R., Emerson, R. W., Klohr, C. L., Adams, C. M., Estes, A. M., Zwaigenbaum, L., Botteron, K. N., McKinstry, R. C., Constantino, J. N., Evans, A. C., … Pruett, J. R., Jr. (2018). Walking, Gross Motor Development, and Brain Functional Connectivity in Infants and Toddlers. *Cerebral Cortex*, *28*(2), 750–763. https://doi.org/10.1093/cercor/bhx313

Mesulam, M. (1998). From sensation to cognition. *Brain*, *121*(6), 1013–1052. https://doi.org/10.1093/brain/121.6.1013

Mitra, A., Snyder, A. Z., Tagliazucchi, E., Laufs, H., Elison, J., Emerson, R. W., Shen, M. D., Wolff, J. J., Botteron, K. N., Dager, S., Estes, A. M., Evans, A., Gerig, G., Hazlett, H. C., Paterson, S. J., Schultz, R. T., Styner, M. A., Zwaigenbaum, L., Network, T. I., … Raichle, M. (2017). Resting-state fMRI in sleeping infants more closely resembles adult sleep than adult wakefulness. *PLOS ONE*, *12*(11), e0188122. https://doi.org/10.1371/journal.pone.0188122

Molloy, M. F., & Saygin, Z. M. (2022). Individual variability in functional organization of the neonatal brain. *NeuroImage*, *253*, 119101. https://doi.org/10.1016/j.neuroimage.2022.119101

Moore, L. A., Hermosillo, R. J. M., Feczko, E., Moser, J., Koirala, S., Allen, M. C., Buss, C., Conan, G., Juliano, A. C., Marr, M., Miranda-Dominguez, O., Mooney, M., Myers, M., Rasmussen, J., Rogers, C. E., Smyser, C. D., Snider, K., Sylvester, C., Thomas, E., … Graham, A. M. (2024). Towards personalized precision functional mapping in infancy. *Imaging Neuroscience*, *2*, 1–20. https://doi.org/10.1162/imag_a_00165

Mueller, S., Wang, D., Fox, M. D., Yeo, B. T. T., Sepulcre, J., Sabuncu, M. R., Shafee, R., Lu, J., & Liu, H. (2013). Individual Variability in Functional Connectivity Architecture of the Human Brain. *Neuron*, *77*(3), 586–595. https://doi.org/10.1016/j.neuron.2012.12.028

Myers, M. J., Labonte, A. K., Gordon, E. M., Laumann, T. O., Tu, J. C., Wheelock, M. D., Nielsen, A. N., Schwarzlose, R. F., Camacho, M. C., Alexopoulos, D., Warner, B. B., Raghuraman, N., Luby, J. L., Barch, D. M., Fair, D. A., Petersen, S. E., Rogers, C. E., Smyser, C. D., & Sylvester, C. M. (2024). Functional parcellation of the neonatal cortical surface. *Cerebral Cortex*, *34*(2), bhae047. https://doi.org/10.1093/cercor/bhae047

Nielsen, A. N., Kaplan, S., Meyer, D., Alexopoulos, D., Kenley, J. K., Smyser, T. A., Wakschlag, L. S., Norton, E. S., Raghuraman, N., Warner, B. B., Shimony, J. S., Luby, J. L., Neil, J. J.,

Petersen, S. E., Barch, D. M., Rogers, C. E., Sylvester, C. M., & Smyser, C. D. (2022). Maturation of large-scale brain systems over the first month of life. *Cerebral Cortex*, bhac242. https://doi.org/10.1093/cercor/bhac242

Ojemann, J. G., Akbudak, E., Snyder, A. Z., McKinstry, R. C., Raichle, M. E., & Conturo, T. E. (1997). Anatomic Localization and Quantitative Analysis of Gradient Refocused Echo-Planar fMRI Susceptibility Artifacts. *NeuroImage*, *6*(3), 156–167. https://doi.org/10.1006/nimg.1997.0289

Petersen, S. E., & Sporns, O. (2015). Brain Networks and Cognitive Architectures. *Neuron*, *88*(1), 207–219. https://doi.org/10.1016/j.neuron.2015.09.027

Power, J. D., Barnes, K. A., Snyder, A. Z., Schlaggar, B. L., & Petersen, S. E. (2012). Spurious but systematic correlations in functional connectivity MRI networks arise from subject motion. *NeuroImage*, *59*(3), 2142–2154. https://doi.org/10.1016/j.neuroimage.2011.10.018

Power, J. D., Cohen, A. L., Nelson, S. M., Wig, G. S., Barnes, K. A., Church, J. A., Vogel, A. C., Laumann, T. O., Miezin, F. M., Schlaggar, B. L., & Petersen, S. E. (2011). Functional Network Organization of the Human Brain. *Neuron*, *72*(4), 665–678. https://doi.org/10.1016/j.neuron.2011.09.006

Power, J. D., Mitra, A., Laumann, T. O., Snyder, A. Z., Schlaggar, B. L., & Petersen, S. E. (2014). Methods to detect, characterize, and remove motion artifact in resting state fMRI. *NeuroImage*, *84*, 320–341. https://doi.org/10.1016/j.neuroimage.2013.08.048

Power, J. D., Plitt, M., Kundu, P., Bandettini, P. A., & Martin, A. (2017). Temporal interpolation alters motion in fMRI scans: Magnitudes and consequences for artifact detection. *PLoS ONE*, *12*(9), e0182939. https://doi.org/10.1371/journal.pone.0182939

Power, J. D., Schlaggar, B. L., Lessov-Schlaggar, C. N., & Petersen, S. E. (2013). Evidence for Hubs in Human Functional Brain Networks. *Neuron*, *79*(4), 798–813. https://doi.org/10.1016/j.neuron.2013.07.035

Raju, H., & Tadi, P. (2024). Neuroanatomy, Somatosensory Cortex. In *StatPearls*. StatPearls Publishing. http://www.ncbi.nlm.nih.gov/books/NBK555915/

Rosvall, M., & Bergstrom, C. T. (2008). Maps of random walks on complex networks reveal community structure. *Proceedings of the National Academy of Sciences*, *105*(4), 1118–1123. https://doi.org/10.1073/pnas.0706851105

Rosvall, M., & Bergstrom, C. T. (2010). Mapping Change in Large Networks. *PLoS ONE*, *5*(1), e8694. https://doi.org/10.1371/journal.pone.0008694

Rousseeuw, P. J. (1987). Silhouettes: A graphical aid to the interpretation and validation of cluster analysis. *Journal of Computational and Applied Mathematics*, *20*, 53–65. https://doi.org/10.1016/0377-0427(87)90125-7

Rudolph, M. D., Graham, A. M., Feczko, E., Miranda-Dominguez, O., Rasmussen, J. M., Nardos, R., Entringer, S., Wadhwa, P. D., Buss, C., & Fair, D. A. (2018). Maternal IL-6 during pregnancy can be estimated from newborn brain connectivity and predicts future working memory in offspring. *Nature Neuroscience*, *21*(5), 765–772. https://doi.org/10.1038/s41593-018-0128-y

Seitzman, B. A., Gratton, C., Laumann, T. O., Gordon, E. M., Adeyemo, B., Dworetsky, A., Kraus, B. T., Gilmore, A. W., Berg, J. J., Ortega, M., Nguyen, A., Greene, D. J., McDermott, K. B., Nelson, S. M., Lessov-Schlaggar, C. N., Schlaggar, B. L., Dosenbach, N. U. F., & Petersen,

S. E. (2019). Trait-like variants in human functional brain networks. *Proceedings of the National Academy of Sciences*, *116*(45), 22851–22861. https://doi.org/10.1073/pnas.1902932116

Smith, S. M., Miller, K. L., Salimi-Khorshidi, G., Webster, M., Beckmann, C. F., Nichols, T. E., Ramsey, J. D., & Woolrich, M. W. (2011). Network modelling methods for FMRI. *NeuroImage*, *54*(2), 875–891. https://doi.org/10.1016/j.neuroimage.2010.08.063

Smyser, C. D., Inder, T. E., Shimony, J. S., Hill, J. E., Degnan, A. J., Snyder, A. Z., & Neil, J. J. (2010). Longitudinal Analysis of Neural Network Development in Preterm Infants. *Cerebral Cortex*, *20*(12), 2852–2862. https://doi.org/10.1093/cercor/bhq035

Sun, L., Zhao, T., Liang, X., Xia, M., Li, Q., Liao, X., Gong, G., Wang, Q., Pang, C., Yu, Q., Bi, Y., Chen, P., Chen, R., Chen, Y., Chen, T., Cheng, J., Cheng, Y., Cui, Z., Dai, Z., … He, Y. (2023). *Functional connectome through the human life span* (p. 2023.09.12.557193). bioRxiv. https://doi.org/10.1101/2023.09.12.557193

Sydnor, V. J., Larsen, B., Bassett, D. S., Alexander-Bloch, A., Fair, D. A., Liston, C., Mackey, A. P., Milham, M. P., Pines, A., Roalf, D. R., Seidlitz, J., Xu, T., Raznahan, A., & Satterthwaite, T. D. (2021). Neurodevelopment of the association cortices: Patterns, mechanisms, and implications for psychopathology. *Neuron*, *109*(18), 2820–2846. https://doi.org/10.1016/j.neuron.2021.06.016

Sylvester, C. M., Kaplan, S., Myers, M. J., Gordon, E. M., Schwarzlose, R. F., Alexopoulos, D., Nielsen, A. N., Kenley, J. K., Meyer, D., Yu, Q., Graham, A. M., Fair, D. A., Warner, B. B., Barch, D. M., Rogers, C. E., Luby, J. L., Petersen, S. E., & Smyser, C. D. (2022). Network-specific selectivity of functional connections in the neonatal brain. *Cerebral Cortex*, bhac202. https://doi.org/10.1093/cercor/bhac202

Tagliazucchi, E., Von Wegner, F., Morzelewski, A., Brodbeck, V., & Laufs, H. (2012). Dynamic BOLD functional connectivity in humans and its electrophysiological correlates. *Frontiers in Human Neuroscience*, *6*. https://www.frontiersin.org/articles/10.3389/fnhum.2012.00339

Talairach, J., & Tournoux, P. (1988). *Co-planar Stereotaxic Atlas of the Human Brain: 3-dimensional Proportional System : an Approach to Cerebral Imaging*. G. Thieme.

Thomason, M. E., Brown, J. A., Dassanayake, M. T., Shastri, R., Marusak, H. A., Hernandez-Andrade, E., Yeo, L., Mody, S., Berman, S., Hassan, S. S., & Romero, R. (2014). Intrinsic Functional Brain Architecture Derived from Graph Theoretical Analysis in the Human Fetus. *PLOS ONE*, *9*(5), e94423. https://doi.org/10.1371/journal.pone.0094423

Thomason, M. E., Dassanayake, M. T., Shen, S., Katkuri, Y., Alexis, M., Anderson, A. L., Yeo, L., Mody, S., Hernandez-Andrade, E., Hassan, S. S., Studholme, C., Jeong, J.-W., & Romero, R. (2013). Cross-Hemispheric Functional Connectivity in the Human Fetal Brain. *Science Translational Medicine*, *5*(173). https://doi.org/10.1126/scitranslmed.3004978

Tooley, U. A., Latham, A., Kenley, J. K., Alexopoulos, D., Smyser, T., Warner, B. B., Shimony, J. S., Neil, J. J., Luby, J. L., Barch, D. M., Rogers, C. E., & Smyser, C. D. (2023). *Prenatal environment is associated with the pace of cortical network development over the first three years of life* [Preprint]. Neuroscience. https://doi.org/10.1101/2023.08.18.552639

Truzzi, A., & Cusack, R. (2023). The development of intrinsic timescales: A comparison between the neonate and adult brain. *NeuroImage*, *275*, 120155. https://doi.org/10.1016/j.neuroimage.2023.120155

Tu, J. C., Myers, M., Sylvester, C., Gordon, E. M., Laumann, T. O., Kardan, O., Feczko, E., Kaplan, S., Day, T. K. M., Miranda-Dominguez, O., Moore, L. A., Sung, S., Chamberlain, T. A., Snider, K., Fair, D. A., Rosenberg, M. D., Elison, J. T., Smyser, C. D., Eggebrecht, A. T., & Wheelock, M. D. (2023, June). *Developing and benchmarking functional parcellations in infant neuroimaging datasets*. Organization for Human Brain Mapping, Montreal, Canada.

Turk, E., Heuvel, M. I. van den, Benders, M. J., Heus, R. de, Franx, A., Manning, J. H., Hect, J. L., Hernandez-Andrade, E., Hassan, S. S., Romero, R., Kahn, R. S., Thomason, M. E., & Heuvel, M. P. van den. (2019). Functional Connectome of the Fetal Brain. *Journal of Neuroscience*, *39*(49), 9716–9724. https://doi.org/10.1523/JNEUROSCI.2891-18.2019

van den Heuvel, M. P., Kersbergen, K. J., de Reus, M. A., Keunen, K., Kahn, R. S., Groenendaal, F., de Vries, L. S., & Benders, M. J. N. L. (2015). The Neonatal Connectome During Preterm Brain Development. *Cerebral Cortex*, *25*(9), 3000–3013. https://doi.org/10.1093/cercor/bhu095

Van Essen, D. C., Drury, H. A., Dickson, J., Harwell, J., Hanlon, D., & Anderson, C. H. (2001). An Integrated Software Suite for Surface-based Analyses of Cerebral Cortex. *Journal of the American Medical Informatics Association*, *8*(5), 443–459. https://doi.org/10.1136/jamia.2001.0080443

Van Essen, D. C., Glasser, M. F., Dierker, D. L., Harwell, J., & Coalson, T. (2012). Parcellations and Hemispheric Asymmetries of Human Cerebral Cortex Analyzed on Surface-Based Atlases. *Cerebral Cortex*, *22*(10), 2241–2262. https://doi.org/10.1093/cercor/bhr291

Wang, D., Buckner, R. L., Fox, M. D., Holt, D. J., Holmes, A. J., Stoecklein, S., Langs, G., Pan, R., Qian, T., Li, K., Baker, J. T., Stufflebeam, S. M., Wang, K., Wang, X., Hong, B., & Liu, H. (2015). Parcellating cortical functional networks in individuals. *Nature Neuroscience*, *18*(12), Article 12. https://doi.org/10.1038/nn.4164

Wang, F., Zhang, H., Wu, Z., Hu, D., Zhou, Z., Girault, J. B., Wang, L., Lin, W., & Li, G. (2023). Fine-grained functional parcellation maps of the infant cerebral cortex. *eLife*, *12*, e75401. https://doi.org/10.7554/eLife.75401

Wen, X., Hsu, L., Lin, W., Zhang, H., & Shen, D. (2020). Co-evolution of Functional Brain Network at Multiple Scales during Early Infancy. *arXiv:2009.06899 [Cs, q-Bio]*. http://arxiv.org/abs/2009.06899

Wen, X., Zhang, H., Li, G., Liu, M., Yin, W., Lin, W., Zhang, J., & Shen, D. (2019). First-year development of modules and hubs in infant brain functional networks. *NeuroImage*, *185*, 222–235. https://doi.org/10.1016/j.neuroimage.2018.10.019

Wheelock, M. D., Hect, J. L., Hernandez-Andrade, E., Hassan, S. S., Romero, R., Eggebrecht, A. T., & Thomason, M. E. (2019). Sex differences in functional connectivity during fetal brain development. *Developmental Cognitive Neuroscience*, *36*, 100632. https://doi.org/10.1016/j.dcn.2019.100632

Wig, G. S. (2017). Segregated Systems of Human Brain Networks. *Trends in Cognitive Sciences*, *21*(12), 981–996. https://doi.org/10.1016/j.tics.2017.09.006

Yates, T. S., Ellis, C. T., & Turk-Browne, N. B. (2023). Functional networks in the infant brain during sleep and wake states. *Cerebral Cortex*, bhad327. https://doi.org/10.1093/cercor/bhad327

Yeo, B. T. T., Krienen, F. M., Sepulcre, J., Sabuncu, M. R., Lashkari, D., Hollinshead, M., Roffman, J. L., Smoller, J. W., Zöllei, L., Polimeni, J. R., Fischl, B., Liu, H., & Buckner, R. L. (2011). The organization of the human cerebral cortex estimated by intrinsic functional connectivity. *Journal of Neurophysiology*, *106*(3), 1125–1165. https://doi.org/10.1152/jn.00338.2011

Supplementary Materials

Supplementary Results

S1. Silhouette index of adult networks in infant FC with the mean in all alternative networks

When the SI was calculated with respect to the mean in all alternative networks rather than the mean of the best alternative network, they were still moderately correlated with the SI reported in the main results (Pearson's r = 0.74, p <0.001). However, since the mean of similarity to all alternative networks (especially to the ones spatially distant from the area in question) would tend to be lower than the best alternative, the SI is positively shifted with almost all parcels having SI > 0 (Supplementary Figure 5).

S2. Age effect on within-network FC is smaller in magnitude with the subset of areas in the Gordon network

If the subset of areas with adult-like network configuration tends to be more stable across infant development, then they will have a relatively stable within-network FC across chronological age. We computed within-network FC across age using full versus subset of areas. For the eight networks that were partially retained, five networks demonstrated a significant correlation between within-network FC and age ($p < 0.05$, Spearman's ρ): the within-network Aud, SMN hand and Vis networks were negatively correlated with age and the within-network FC in DAN and the FPN were positively correlated with age. The age effect was greater in magnitude with the full set of areas (Figure 3A) than with only the partially retained areas (Figure 3B) for the SMN hand network, although not significant when comparing the Fisher-Z-transformed ρ values ($Z = 1.588$, one-sided p = 0.056). Similar results were found for other networks, where the age effect was less negative for Aud, SMN hand and Vis networks, and less positive for DAN and FPN, but none of them had a significant ($p < 0.05$) Z-test. To examine the robustness of our result to the selection of data samples, we generated 1000 bootstrapped samples of the infant sessions. We found that the sign of the difference was consistent across bootstrap samples (i.e., on average the networks using the subset of areas were less correlated with age than the full set of areas) (Figure 3C). The mean and 95% confidence interval for the bootstrap showed a mean difference in Fisher-Z-transformed ρ values for full versus subset was -0.1139 [-0.1721,0.0129] for Aud, -0.1386 [-0.1684, -0.0814] for SMN hand, 0.0020 [-0.0887, 0.0348] for Vis, -0.0205 [-0.0120, 0.1439] for DAN and 0.0089 [0.0071, 0.0511] for FPN (Figure 3C).

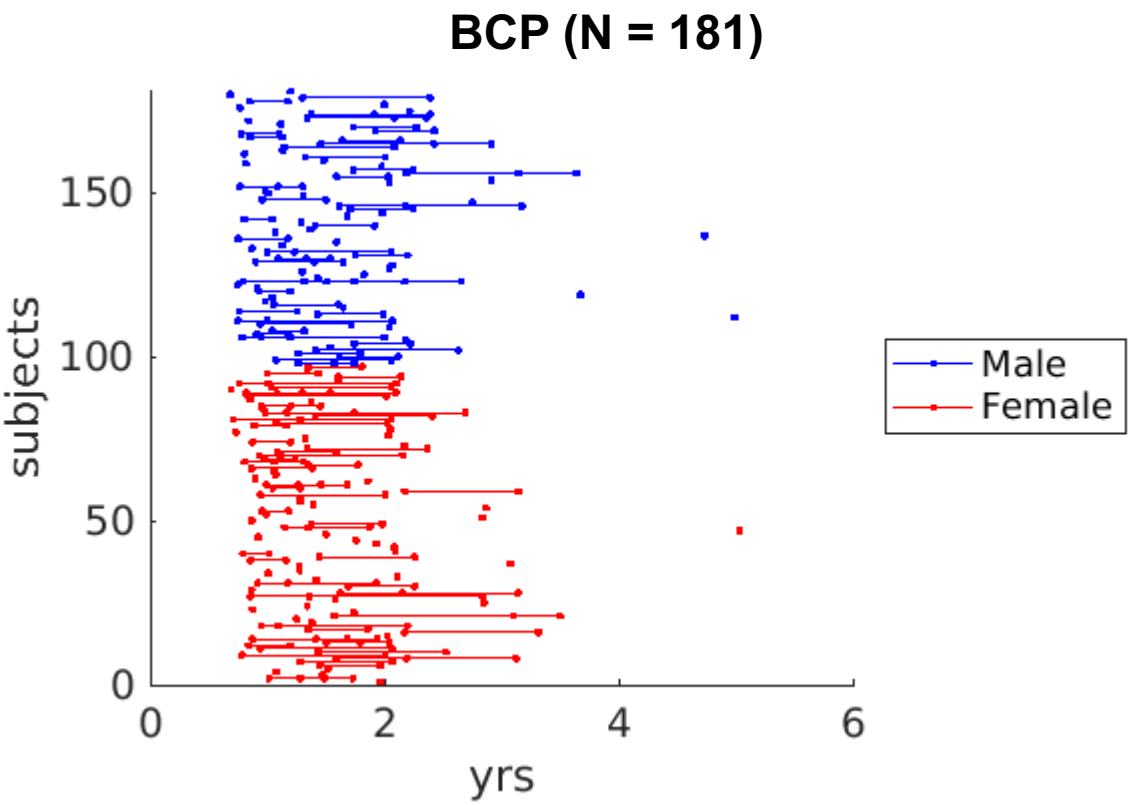

Supplementary Figure 1. *Distribution of age and sex*

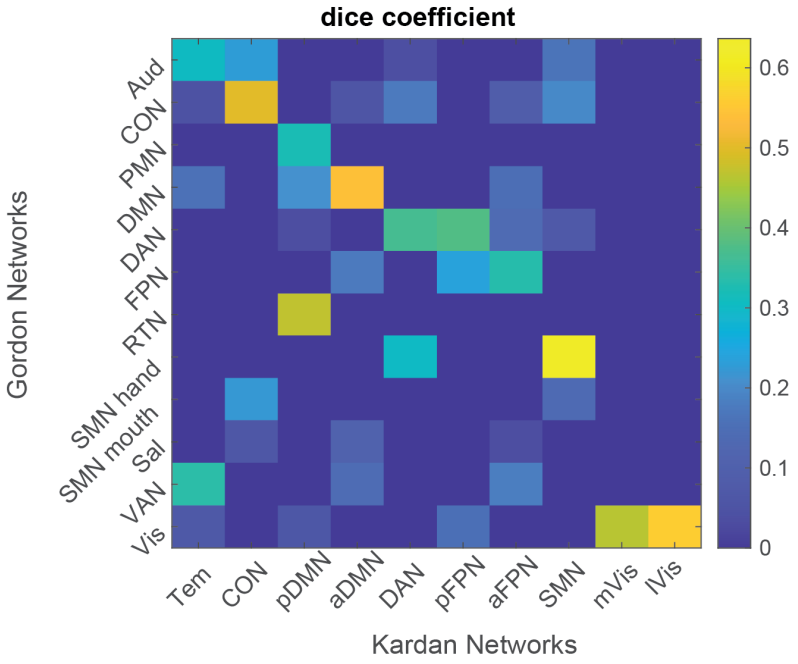

Supplementary Figure 2. *Dice overlap between the Gordon Networks (Adult) and the Kardan Networks (Infant).* Network abbreviations: auditory (Aud), cingulo-opercular (CON), parietal memory (PMN), default mode (DMN), dorsal attention (DAN), fronto-parietal (FPN), retrosplenial temporal (RTN), somatomotor hand (SMN hand), somatomotor mouth (SMN mouth), salience (Sal), and ventral attention (VAN), visual (Vis), somatomotor (SMN), temporal (Tem), posterior frontoparietal (pFPN), posterior default mode (pDMN), lateral visual (lVis), medial visual (mVis), anterior fronto-parietal (aFPN), anterior default mode (aDMN).

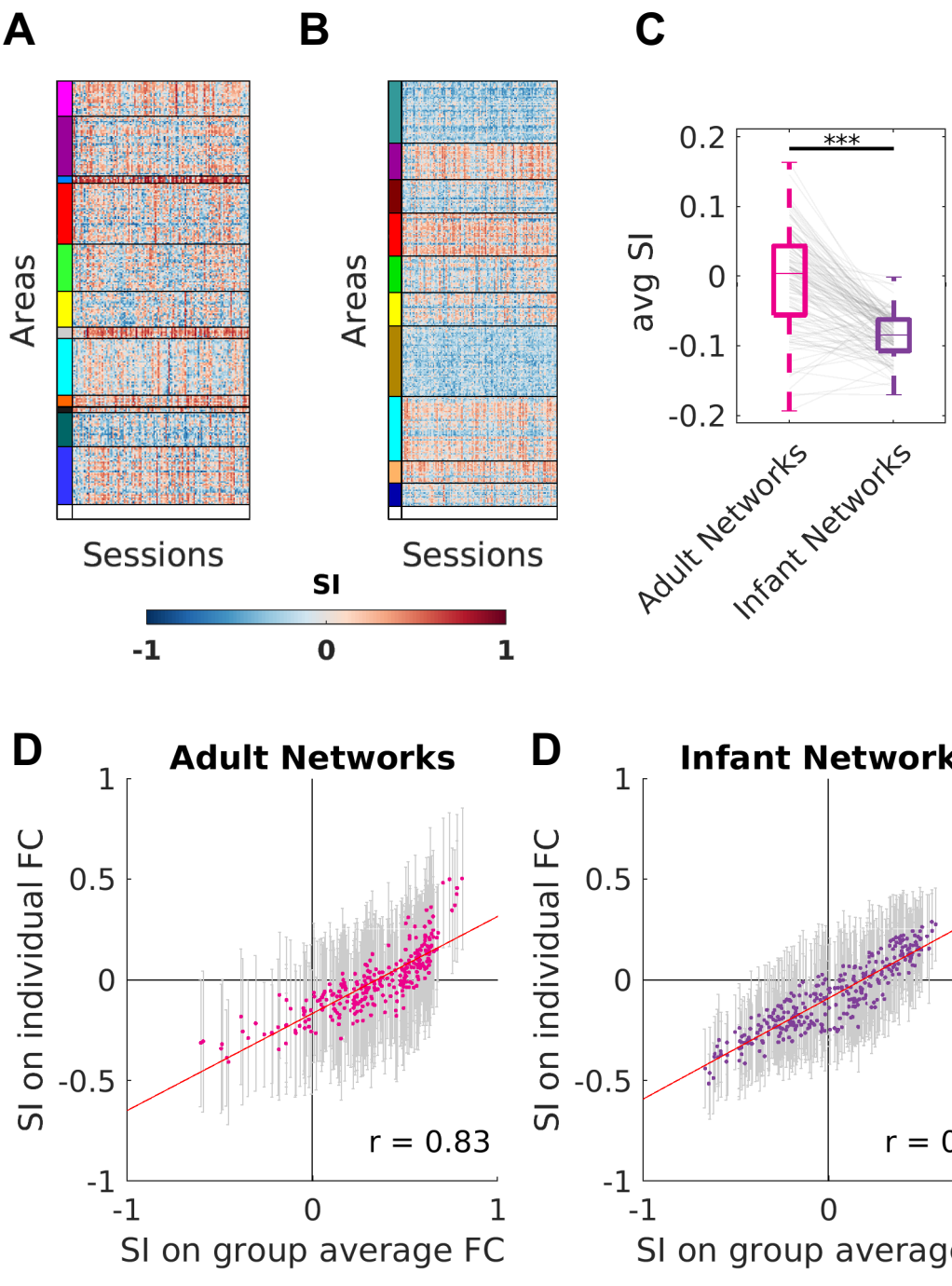

Supplementary Figure 3. *Silhouette index (SI) of adult and infant networks on individual adults' FC.* A) SI across adult networks (Gordon, 286 areas). B) SI across infant networks (Kardan, 328 areas). C) average SI of adult and infant networks across areas on individual adults' FC. *** $p < 0.001$ in paired t-test. D) Pearson's correlation of SI of adult networks on group average FC and the mean of SI on individual FC across 286 areas. E) Pearson's correlation of SI of infant networks on group average FC and the mean of SI on individual FC across 328 areas.

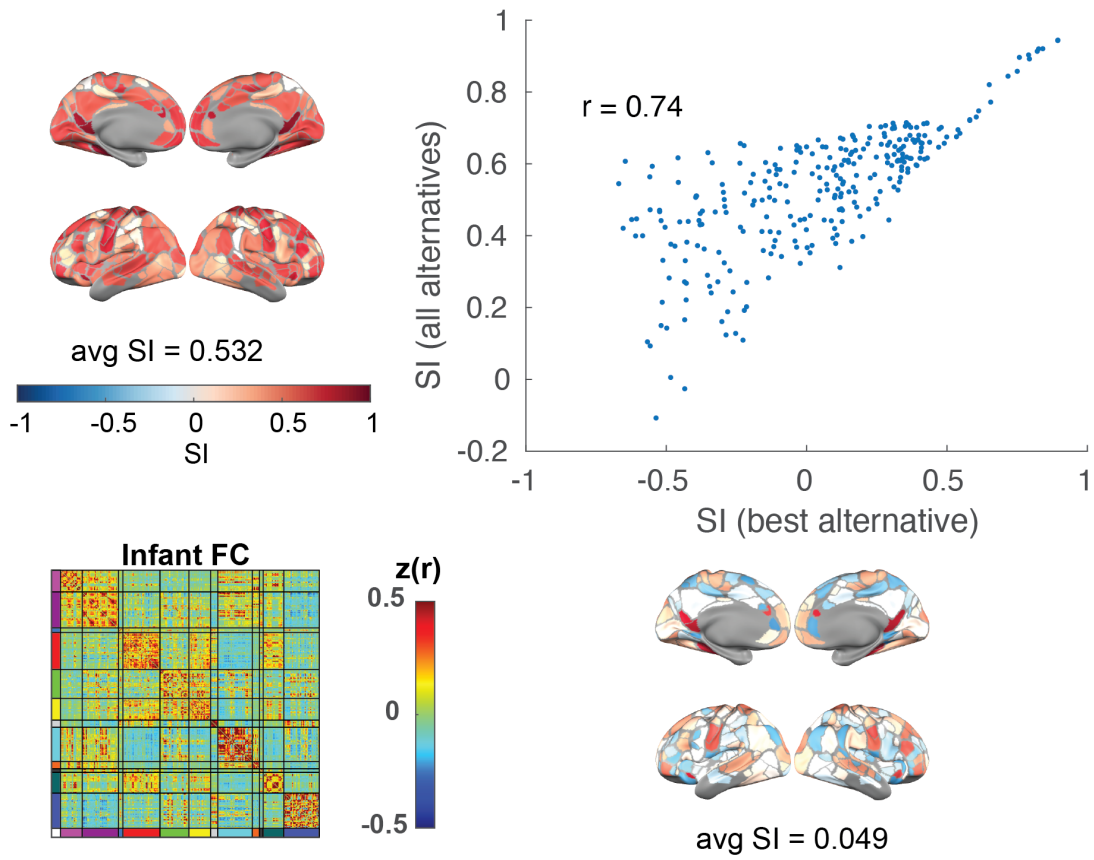

Supplementary Figure 5. *Correlation between silhouette index calculated with the best network or with all alternative networks*.

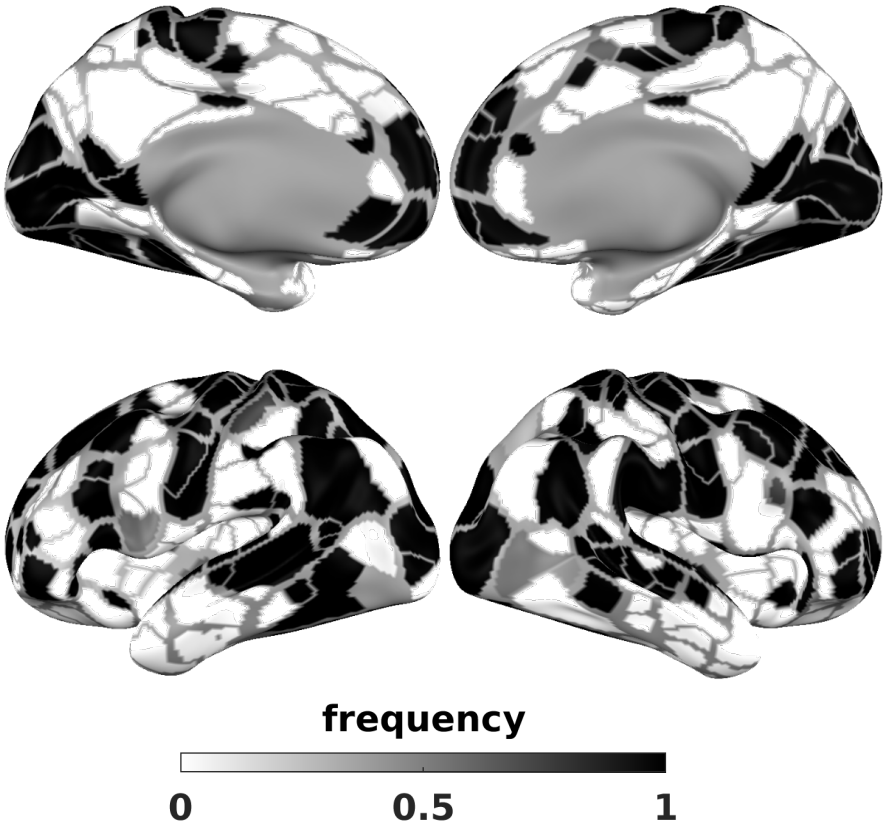

Supplementary Figure 6. *Frequency of SI > 0 across 1000 bootstraps.*

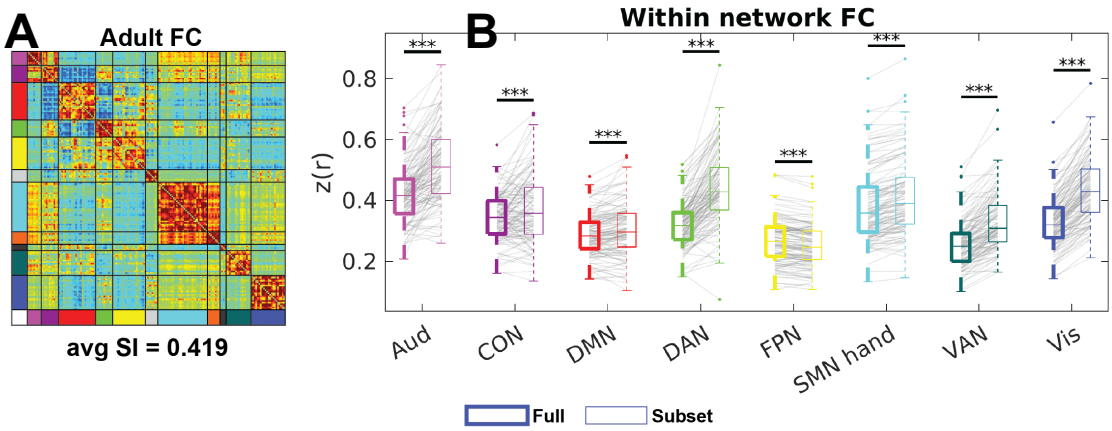

Supplementary Figure 7. *Adult FC using the Gordon Subset.* A) The sorted average FC in infants with the subset of areas. B) The average within-network FC with full (left) versus subset (right) across sessions.

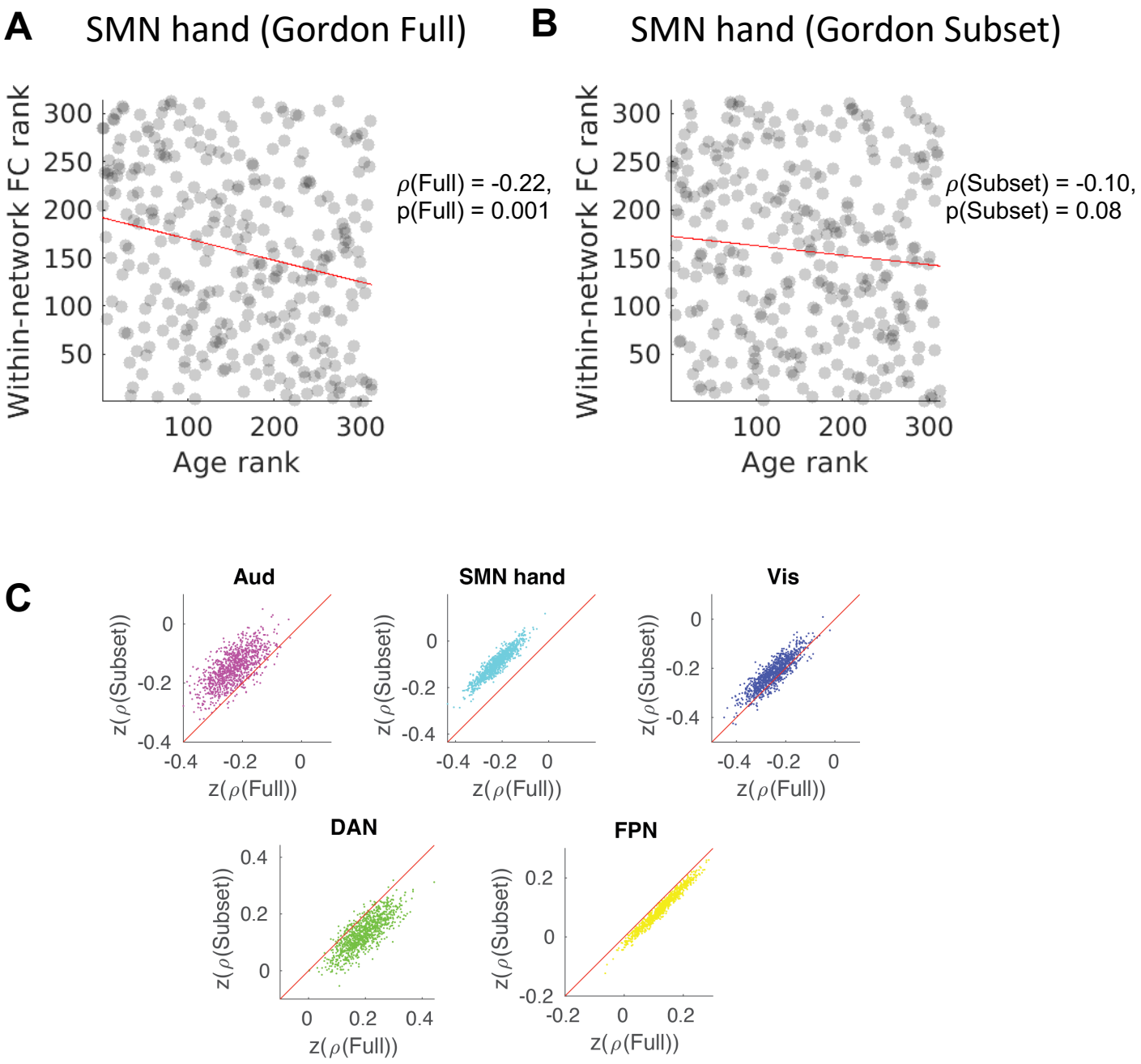

Supplementary Figure 8. *Correlation between age and within-network FC in using the subset of areas versus the full set of areas.* A) Scatter plot of within-network FC versus age for SMN hand network defined with the full set of areas. B) Scatter plot of within-network FC versus age for SMN hand network defined with the subset set of areas. C) The within-network FC for three networks is negatively correlated with age (Aud, SMN hand, Vis), and the within-network FC for two networks is positively correlated with age (DAN, FPN). The x-axis is the Fisher-Z-transformed Spearman's correlation (ρ) between within-network FC using the full set of areas and age. The y-axis is the Fisher-Z-transformed Spearman's correlation (ρ) within-network FC using the subset of areas and age). Each data point represents a bootstrap sample of sessions (N = 1000). Red line shows the line of least-squared fit in A-B and the line of identity in C.

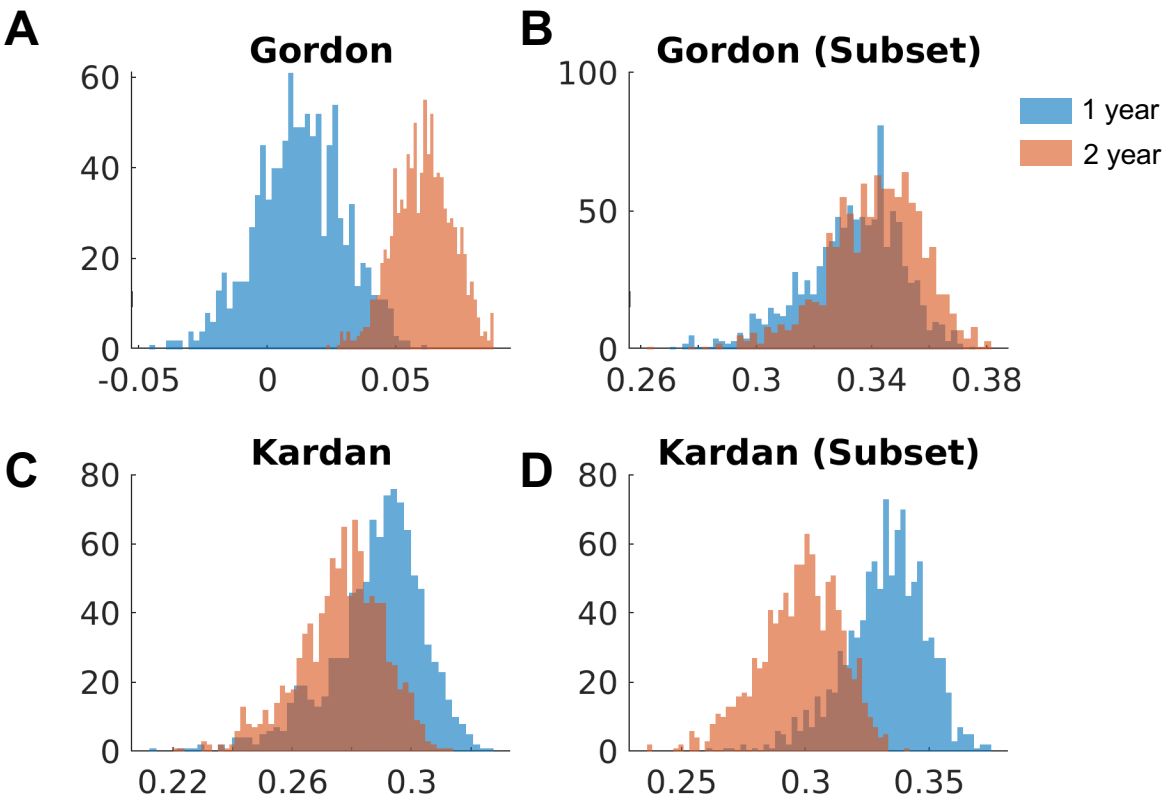

Supplementary Figure 9. *Bootstrapped distributions of average silhouette Index at 1 year and 2 years (N = 1000 bootstrapped samples).* A) Gordon networks. B) Gordon networks but with the subset of areas in Figure 2A. C) Kardan networks. D) Kardan networks but with the subset of areas in Figure 2A.

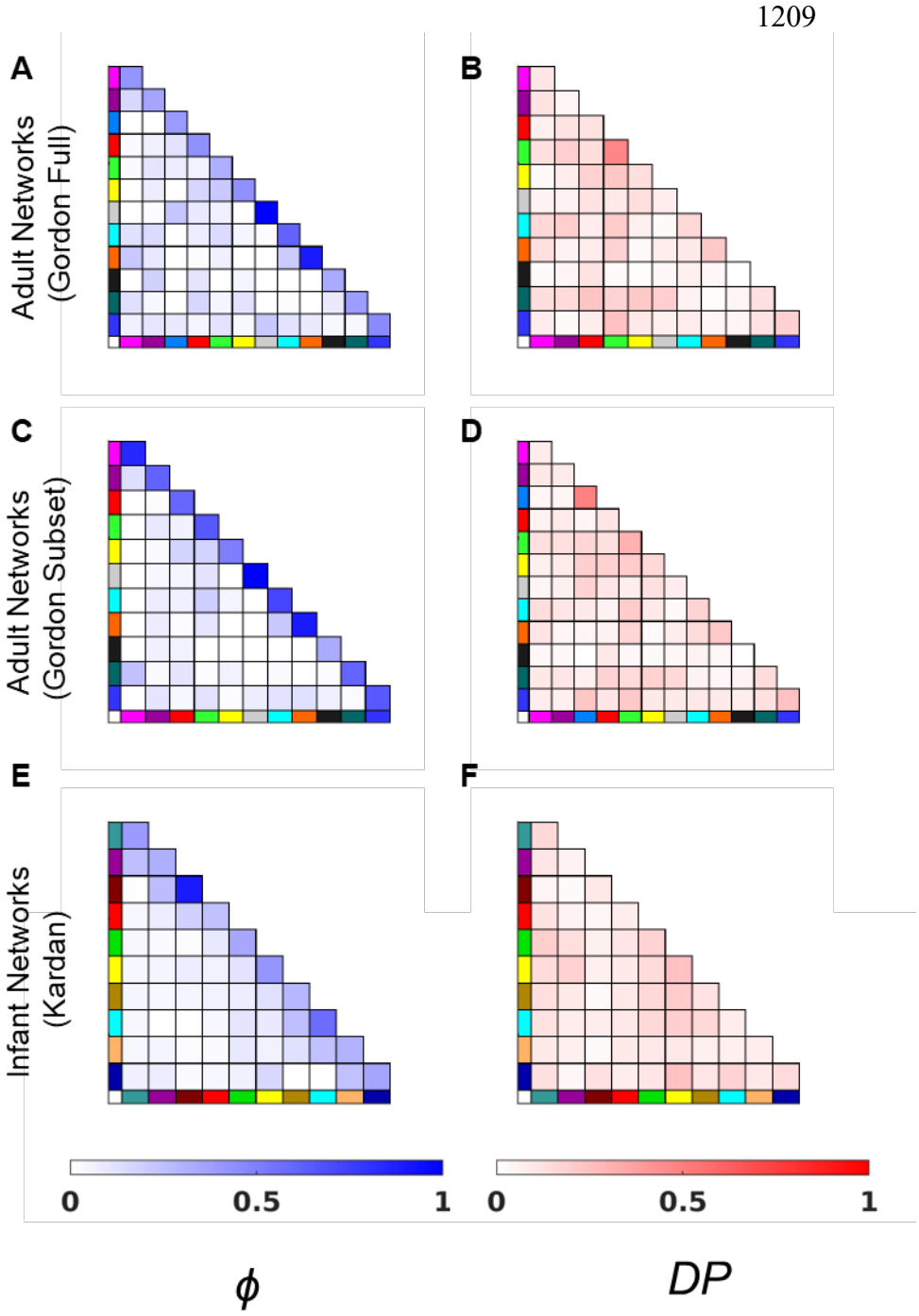

Supplementary Figure 10. *Fraction of high consistency (ϕ) and high differential power (DP) edges (top 10%) across Gordon Full (A-B), Gordon Subset (C-D), Kardan (E-F).*

1210 **Supplementary Table 1.** Percentage of highly consistent (ϕ) edges across different network assignment schemes

	Gordon Full	Gordon Subset	Kardan
within-network	44.1%	63.1%	49.5%
between-network	8.3%	6.5%	5.4%

1211 **Supplementary Table 2.** Percentage of highly consistent (ϕ) edges across different network assignment schemes. The eight partially retained networks were bolded and had an asterisk.

within-network	Gordon Full	Gordon Subset
Aud*	41.30%	84.21%
CON*	35.64%	61.73%
PMN	40.00%	/
DMN*	43.17%	59.07%
DAN*	31.45%	65.17%
FPN*	43.12%	50.84%
RTN	100%	100%
SMN hand*	61.45%	72.82%
SMN mouth	89.29%	89.29%
Sal	33.33%	33.33%
VAN*	38.34%	60.94%
Vis*	45.89%	65.17%

1212 **Supplementary Table 3.** Percentage of high differential power (*DP*) edges across different network assignment schemes.

	Gordon Full	Gordon Subset	Kardan
within-network	16.50%	14.73%	12.79%
between-network	10.81%	10.98%	9.93%

1213 **Supplementary Table 4.** Percentage of high differential power (*DP*) edges across different network assignment schemes. The eight partially retained networks were bolded and had an asterisk.

within-network	Gordon Full	Gordon Subset
Aud*	7.97%	10.53%
CON*	8.33%	4.94%
PMN	50.00%	/
DMN*	10.73%	11.59%
DAN*	30.24%	47.19%
FPN*	15.58%	13.91%
RTN	7.14%	7.14%
SMN hand*	17.92%	15.82%
SMN mouth	21.43%	21.43%
Sal	0%	0%
VAN*	14.62%	12.02%
Vis*	24.97%	18.43%